UNIVERSITÉ DU QUÉBEC

MÉMOIRE PRÉSENTÉ À

L'UNIVERSITÉ DU QUÉBEC À CHICOUTIMI

COMME EXIGENCE PARTIELLE

DE LA MAÎTRISE EN INGÉNIERIE

Par

MAHIN DERAKHSHANIAN

SIMULATIONS NUMÉRIQUES DES VIBRATIONS INDUITES PAR EFFET DE COURONNE SUR UN COURT CONDUCTEUR SOUMIS À UNE PLUIE ARTIFICIELLE

August 2001

Mise en garde/Advice

To those who have filled my life with love

My husband, Shahriar; my daughter, Shadi; my son Sherwin and my mother, Fatemeh

CONTENTS

Table of Figures

List of Tables

Résumé

Dans les conditions humides, l'avénement de couronne sur les lignes de transmission haute-tension pourrait aboutir à la vibration des conducteurs. Ce type de vibration, connu comme "Vibration induite par effet de couronne", peut conduire à la fatigue des conducteurs et leurs éléments de support. Il a été établi que la présence intermittente de la charge d'espace de couronne et du vent ionique sont les causes principales de ce phénomène.

L'objectif principal de ce mémoire de maitrise est la simulation numérique et experimentale sur deux conducteurs courts, l'un lisse et l'autre toronné.

Pour la partie expérimentale, notre approche est basée sur un modèle physique déjà employé dans les travaux précédents du GRIEA "Groupe de Recherche de l'Ingénierie de l'Environnement Atmosphérique". Ce modèle utilise un conducteur placé au centre d'un cylindre en grillage métallique. Ce dispositif a permis d'étudier l'influence des différents facteurs sur les vibrations des conducteurs haute-tension placés sous la pluie artificielle. Les résultats des simulations expérimentales seront appliqués au modèle numérique en vue d'effectuer les simulations numériques. La méthode des éléments finis a été utilisée pour développer le modèle numérique.

En vue de valider un modèle pratique avec les résultats expérimentaux, deux modèles numériques ont été développés. Le premier modèle, considéré comme modèle de base est développé pour un conducteur lisse, alors que le deuxième, appliqué au conducteur toronné, a pour but de compléter le modèle de base.

Les entrées pour ces deux modèles numériques sont appliquées au logiciel COSMOS et les simulations ont été exécutées. Les forces impliquées dans la constitution des gouttes d'eau et leur éjection d'un conducteur haute-tension seront modélisées numériquement en utilisant les resultats des travaux de recherches précédents et en sélectionnant la meilleure combinaison de ces forces.

Les résultats expérimentaux sont utilisés pour évaluer la précision des résultats numériques ainsi que leur validation.

Abstract

Under wet conditions, occurrence of corona on high voltage transmission lines could cause vibration of conductors. This kind of vibration, referred to as corona-induced vibration, could lead to fatigue of conductors and supporting elements. It has been established that the intermittent presence of corona space charge and ionic wind are the main causes of this phenomenon.

The main objective of the present Master's thesis is the laboratory and numerical simulations of the corona-induced vibration of short soft and ACSR (Aluminium Conductor Steel Reinforced) conductors.

For the laboratory simulation, a physical model already used in previous works of the Research Group on Atmospheric Environment Engineering (GRIEA), is employed. This model consisting of a conductor placed in the centre of a mesh cage allowed to investigate the influence of different factors on the vibration of high voltage conductors under artificial rain. The results of the experimental simulations are launched to the numerical model to perform the numerical simulations.

Finite Element Method is used to develop the numerical model. To present a practical model that can be validated with experimental results, two numerical models are developed. The first model, considered as a basic model, is developed for a smooth conductor, while the second one, applied to the ACSR conductor, is intended to complement the basic model. The forces involved in the constitution of water drops and their ejection from a high voltage conductor are numerically modelled by using the previous researches and selecting the best

combination of these forces. The inputs for these two numerical models are applied to COSMOS software and the simulations are performed.

To validate the numerical results obtained by the numerical simulations, the experimental results are used to evaluate the accuracy of the numerical results.

Acknowledgement

I take this opportunity to express my thanks to all who have helped me, either for technical or moral support, to finish this thesis.

First of all, I would like to thank my director, Professor Masoud Farzaneh, for his support and supervision for the entire work of my M.A.Sc. studies. I would like to acknowledge my co-director, Professor Gille Bouchard, for his support and guidance and also for his helpful advice and discussions.

I would also like to express my appreciation to the entire staff of the GRIEA, in particular Sylvain Desgagnés, for their help and excellent working atmosphere. I wish to thank Chantale Dumas, secretary of Applied Science Department, for her help and assistance during my studies at UQAC.

Last, but by no means least, my heartfelt thanks go to my dear husband, Shahriar, for his support, advice, patient and love.

CHAPTER 1

INTRODUCTION

1.1. Background

From the beginning of the development of high voltage networks, the attention of engineers and of researchers was attracted to the phenomenon of partial discharge or the corona effect. This phenomenon manifests itself in the form of bluish luminous sheath that appears around aerial high voltage conductors. Research in this field began in 1915 with R.W. Peek [Peek, 1915] by a detailed experimental study on the phenomenon of the corona effect. He established an empirical law expressing the electrical field threshold at which the corona effect appears.

By development of electrical transportation networks, it became apparent that the phenomenon of the corona is also a contribution to radio and audio disturbances, and energy loss. This increased interest given to this topic when design of high voltage aerial lines was being conceived. This economical aspect incited researchers to interest themselves in this phenomenon, to study the mechanisms of partial discharge and especially to be mindful of their consequences.

One of the types of partial discharge on the high voltage transmission lines is reported as corona-induced vibration [Farzaneh, 1986]. This kind of vibration on the transmission line conductors is generally observed under rainfall and in the presence of high electrical field at the surface of the conductors.

1.2. Problem Definition

One of the inevitable consequences of the transportation of energy electric for the high voltages is the apparent of corona effect. It ionizes the air around the high voltage conductor and creates the charge positive and/or negative while intense electrical field is applied. These charges are either attracted or rejected based on the polarity of conductor. The origin of these electrical charges is a contribution to radio and audio disturbances, and energy loss. While tendency of new technology is towards increment of transportation voltage, study on this domain attracts more and more researchers. Consequently, corona discharge on high voltage transmission lines became an important subject for this domain of research.

In 1915, M.F. Peek introduced the effect of corona on high voltage conductors, which are under rain, as a vibration on transmission lines [Peek, 1915]. Based on literature [Farzaneh, 1986], this kind of vibration appears when the gradient of superficial voltage exceeds 16 kV/cm. The frequency of vibration is reported in a range of 1 to 5 Hz with a peek to peek amplitude of 10 cm [Farzaneh, 1986] [Demers, 1994].

It is now about two decades that University of Quebec in Chicoutimi (UQAC) is leading the study on the corona-induced vibration [Farzaneh, Phan, 1984]. During these years many of researchers have studied the different aspects of this subject. Diverse experimental models and laboratory mechanisms are used to simulate this phenomenon. However the most of researchers accomplished the successive results but least of these results are based on a numerical model and numerical simulation. For this reason the present research is based on the both numerical and experimental simulations of the corona-induced vibration. This vibration has been studied on a short high voltage conductor submitted to

3

artificial rain. The results of the experimental simulation are launched to the numerical model to perform the numerical simulations.

1.3. Bibliography

During the present research work, several papers and theses have been analyzed. The most important of them are as follow:

- ➢ Hara M. and his colleagues introduced modes of corona discharge and specific charge of water drops as well as formation of water drops in various electrical fields. The main purpose of this work was to show experimentally the relationship between the modes of corona discharge (no-corona, crackling corona, hissing corona, and wire corona) and the dripping manner of water drops from a high voltage conductor and their threshold conditions.

- ➢ Shah & Morgan used finite element methods for numerical simulation of vibrations induced by corona on transmission lines. It seems that they have been the first group which employed a numerical simulation approach for this phenomenon.

- ➢ Experimental results presented by M. Farzaneh are as a worthful thesaurus for researchers in this domain. Some of his results are reviewed in this research work.

- ➢ Maaroufi presented the mathematical models of the applied forces on water drops, suspended under a high voltage conductor in his research work.

- ➢ P. Demers' thesis is a base for this research work. Methodology of his numerical simulation is explained in detail in chapter three.

1.4. Objectives

The principal objectives of this thesis are considered as follows:

➤ Experimental simulation of the corona-induced vibration on a smooth conductor supplied by high voltage and placed under the artificial rain.

➤ Experimental simulation of the corona-induced vibration on the ACSR (Aluminum Conductor Steel Reinforced) conductor supplied by high voltage and placed under the artificial rain.

➤ Presentation of numerical models for the forces involved in corona-induced vibration of high voltage conductors.

➤ Presentation of a numerical model for the corona-induced vibration on the mentioned situation.

➤ Numerical simulations of the vibrations, induced by corona on the high voltage conductors, for smooth and ACSR conductors.

➤ Validation of the numerical results by the experimental results.

1.5. Methodology

The experimental model, installed in Physic of Discharge Laboratory of GRIEA [Farzaneh, 1986] is used in this research work to explore the characteristics of the vibration induced by corona effect on a short conductor submitted to artificial rain. This model provides a facility to investigate the influence of different factors on the vibration of high voltage conductors under rain. The results of the experimental simulations are launched to the numerical model to perform the numerical simulations.

5

The forces involved in the constitution of water drops and their ejection from a high voltage conductor is numerically modeled by using the previous researches and selection of the best combination of these forces.

In this research, the *Finite Element Method* is used to develop the numerical model for the corona-induced vibration on a short conductor submitted to artificial rain. To present a practical model that can be validated with experimental results, two numerical models are designed. The first design models a smooth conductor to represent a basic model for this kind of vibration, and the second one uses an ACSR conductor to complement the first model and take a better approach in order to model the conductors on the transmission lines more precisely. The inputs for these two numerical models are applied to COSMOS software and the simulations are performed. To obtain the numerical results, the Post-Processing step is employed.

To validate the numerical results obtained by the numerical simulations, the experimental results are used to evaluate the precision of the numerical models and the suitability of the numerical method.

1.6. Survey of the Thesis

There are a total of seven chapters in this thesis. In chapter 1, a brief definition of problem, the objectives and the methodology of the work are presented.

Chapter 2 offers a fundamental definition of corona discharge and familiarizes the reader with the basic terminology in this domain. In chapter 3, a review of previous research in this field is presented.

In chapter 4, the experimental models are introduced and the laboratory instruments needed to run the experiences are described. Then two samples of drop profiles are shown and analyzed while the rest of them are displayed in the Appendix. Afterwards, the variations of drop volume on the smooth and the ACSR conductors are interpreted and the experimental results are presented.

Chapter 5 summarizes the method of the numerical simulations and consists of the following sections: Theory of Finite Element, Numerical Model, Numerical Simulations for the Smooth Conductor and the ACSR Conductor, Static Analysis, Dynamic Analysis, and Post-processing Results.

The validation of models and the comparison of the experimental results with the numerical results are presented in chapter 6. Finally in chapter 7, the impact of this work is summarized.

CHAPTER 2

FUNDAMENTAL DEFINITIONS OF

CORONA DISCHARGE

2.1.   Introduction

The objective of this chapter is to introduce basic definition of corona discharge, which gives a facility for understanding the following chapters.

First, ionization in gases is explained briefly. Then corona discharge is described and reviewed. Corona discharge is introduced in three subdivisions:

1) Corona effect at the cathode (negative discharge)

2) Corona effect at the anode (positive discharge)

3) Corona discharge in alternating current

Then in the next section, the speed of electrical wind versus discharge current for one-dimensional electrical fields is formulated. Finally, in the last section, the phenomenon of corona discharge on the transmission lines is interpreted in fair and rainy weather.

2.2.   Ionization in Gases

The phenomenon of ionization can occur during an inelastic collision. This kind of collision arises when an electron of the gas becomes excited or ionized by acquired energy from the incident particle. In fact, whenever conversion from kinetic to potential energy or vice-versa occurs, the collision is inelastic.

Occurrence of inelastic collision in gases and consequently their ionization have been reported by various procedures. However, in most of them different process of production of ions and free electrons are classified as follows:

2.2.1 Ionization by electron impact

In the presence of an electrical field, free electrons become accelerated. These electrons collide with other particles of gas and transfer their kinetic energies. If the energy is sufficient to cause ionization, the electrons are released and the free electrons repeat the same process. The primary free electrons necessary for starting this process are produced by cosmic ray ionization.

2.2.2 Photoionization

Photoionization happens when an excited atom emits a photon. It occurs because the electron returns from a higher level of energy to a lower orbit. The reverse process takes place when an atom absorbs an incident photon by letting an electron move to a further orbit. In order to cause excitation for a photon on a neutral unexcited atom, it must possess energy, $h\nu$ (h Planck constant, ν frequency of the photon), that is at least equal to the lowest excitation energy of the atom.

Excitation occurs when: $\qquad h\nu \geq w_e \qquad$ or $\qquad \lambda \leq ch/w_e$

Ionization occurs when: $\qquad \lambda \leq ch/w_i$

This means that the higher the energy of ionization, the shorter the wavelength of radiation. For example:

$$w_i \quad \text{for Oxygen} = 12.2 \text{ eV}$$

$$w_i \quad \text{for Nitrogen} = 15.5 \text{ eV}$$

2.2.3 Surface phenomenon

A surface phenomenon appears when an electron in the last orbit of a metallic electrode has sufficient energy to cross the potential barrier. Therefore, the free electron exits from the metal crystal network and participates in the electronic conduction in the air.

2.2.4 Formation of negative ions

Negative ions are formed by the attachment of electrons on the neutral molecules of an electronegative gas, such as Oxygen. This phenomenon occurs while the electrons are not energetic. In general, the attachment in the air is stopped when the electrical field exceeds the critical value of 15 kV/cm.

2.3. Corona Discharge

As it is explained in section 2.1, different methods of ionization can produce free electrons, positive ions and consequently the avalanche phenomenon. The successive development of electron avalanches between electrodes can result in breakdown. This breakdown means that the channel conductivity has reached a value high enough to cause the current, theoretically infinite and practically limited by the outer circuit.

The assembly of the phenomena of discharge, which precedes the breakdown, is called corona. For the most part, the stable corona discharge appears when the ambient pressure is high enogh (>20 mmHg) in a non-uniform electrical field.

2.3.1　Corona Effect at the Cathode (Negative Discharge)

Negative discharge appears when the multiplication of charges, produced by the collision of secondary electrons (generated by a primary avalanche) and the molecule of gas, augments the ionization.

Photoionization and electrons emission caused by the bombardment of positive ions at the cathode are the most significant methods of ionization.

➤ **Photoionization**

Photoionization is an active process, because the energy of photons, emitted by an excited Nitrogen atom, is superior to the ionization energy of an Oxygen molecule.

➤ **Bombardment of positive ions at the cathode**

The positive ions of ionization are projected to the cathode by the intensity of an electrical field. This sometime results extracting the electrons from the cathode.

Three different modes of corona discharge at the cathode are as follows:

2.3.1.1 Trichel Impulses

Trichel impulses (Trichel streamers) are observed when the applied field becomes greater than the threshold field of the corona effect. The critical value of the threshold field for a cylindrical configuration has been developed by F.W.Peek [Peek, 1915] as:

$$E_{crit} = E_p \; \delta \cdot \left(1 + \frac{K}{\sqrt{\delta \cdot r}} \right)$$

E_{crit}　　critical field

E_p　　superficial field

K	coefficient K=0,308
r	radius of the conductor
δ	relative density of air

Trichel impulses consist of three zones. These zones are listed below and shown in Figure 2-1.

a) Multiplication of charges by secondary ionization

b) Suppression of discharge by space charges

c) Evacuation of space charges

a) 5 ~ 50 nsec
b) 100 ~ 195 nsec
c) 10 Micro-sec
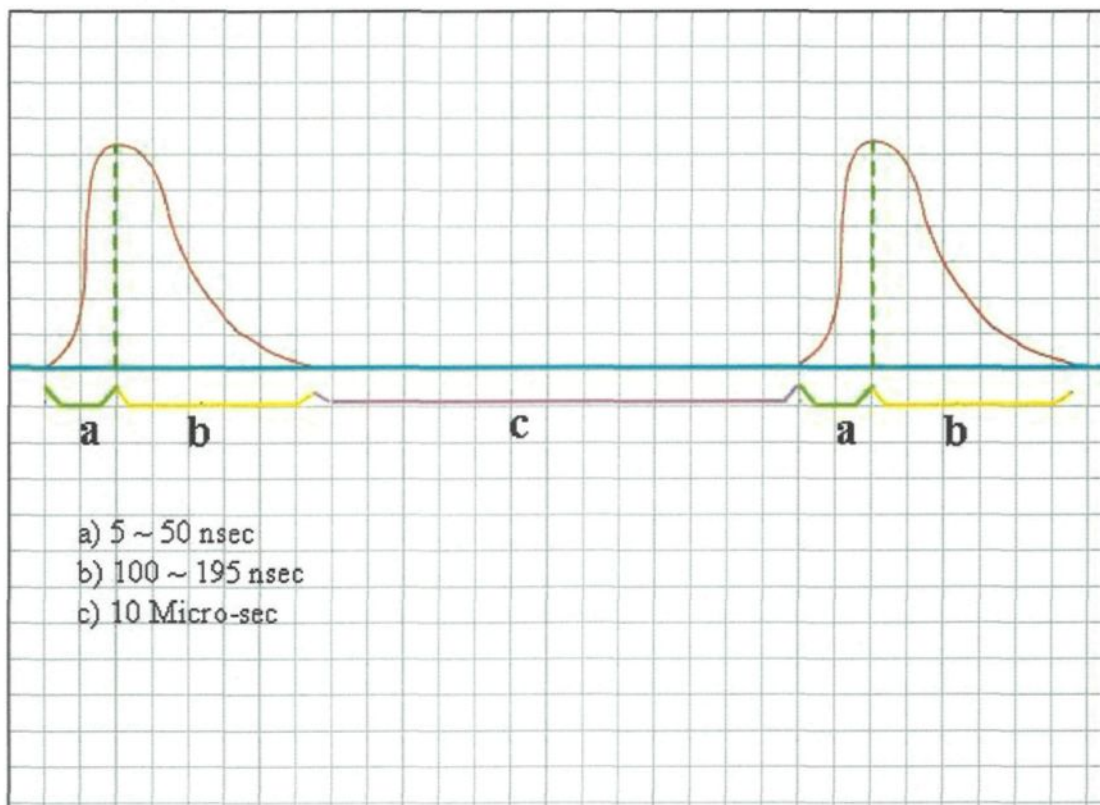
Figure 2-1: Three zones of Trichel impulses

While ionization is intense, the evacuation of ions is slower than electrons. There is an accumulation of space charges in the neighborhood of the cathode. The cathode absorbs the positive ions and an excess negative charge is produced. These produced charges suppress the discharge as the initial electrical field diminishes. Then, the repulsive forces between the cathode and the free electrons repulse the electrons and evacuate the space charges until the situation is ready for the next period.

Luminous cone form, with a short rising and duration time, is the most significant characteristics of these impulses. As reported by Farzaneh [Farzaneh, 1986], the duration time is approximately 150-200 ns and the time distance between two successive impulses is approximately 10 μs.

2.3.1.2 Negative Pulseless Glow

As the electrical field is further increased, the type of discharge current changes and produces a continuous discharge without impulse. Since the space charges cannot be formed any more, the phase "suppression of discharge" does not exist and the negative pulseless glow appears. There exists a critical frequency of Trichel impulses, which is a transitional frequency between these two modes of discharge (Trichel impulses and negative pulseless glow). As reported by Farzaneh, there is a change in the intensity of discharge current at about this transitional frequency (approximately in tens of μA) [Farzaneh, 1986].

The most undesirable effects of corona are radio disturbances, which are produced by discharge impulses. The presence of negative pulseless glow mode on the transmission line continued with negative polarity stops the radio disturbances.

2.3.1.3 Negative Streamers

By increasing the applied voltage, before breakdown and in certain particular configurations (spherical or conical protuberance) another type of discharge is observed, which is called negative streamers [Loeb, 1941].

The existence probability of this mode on the transmission line is low, as this mode occurs only while the voltage is extremely high [Farzaneh, textbook 1992].

2.3.2 Corona Effect at the Anode (Positive Discharge)

The existence electrons in the air moving towards the anode while an avalanche is produced by the secondary ionization. During these displacements, the free electrons are closer to the anode and the electrical field is intense. Consequently, conditions to develop an avalanche are improved. Therefore, the corona field in positive voltages is less than in negative voltages.

Three different modes of corona discharge at the anode are shown in Figure 2-2 and described as follows:

2.3.2.1 The impulses at the beginning of the phenomena

When the applied voltage passes from the threshold value, a luminous discharge appears in the neighborhood of the anode (Figure 2-1, a). This discharge consists of many filaments which are the first visible luminous and are named the impulses at the beginning of the phenomena. Rise time, and duration time of these pulses are greater than for the Trichel impulses.

2.3.2.2 Hermstein Glow

An intensive electrical field changes the type of discharge from the initial impulses to the stable glows, which adhere to the surface of electrodes (Figure 2-1, b). For an electrode with a typical geometry, the interval time of the Hermstein pulses is ten times greater than the interval time of the initial impulses.

2.3.2.3 Streamers

After observing the Hermstein glows, and if the applied voltage is further increased, streamers will begin to appear (Figure 2-1, c). These streamers are the same as the initial impulses, but are longer and stronger [Loeb, 1965].
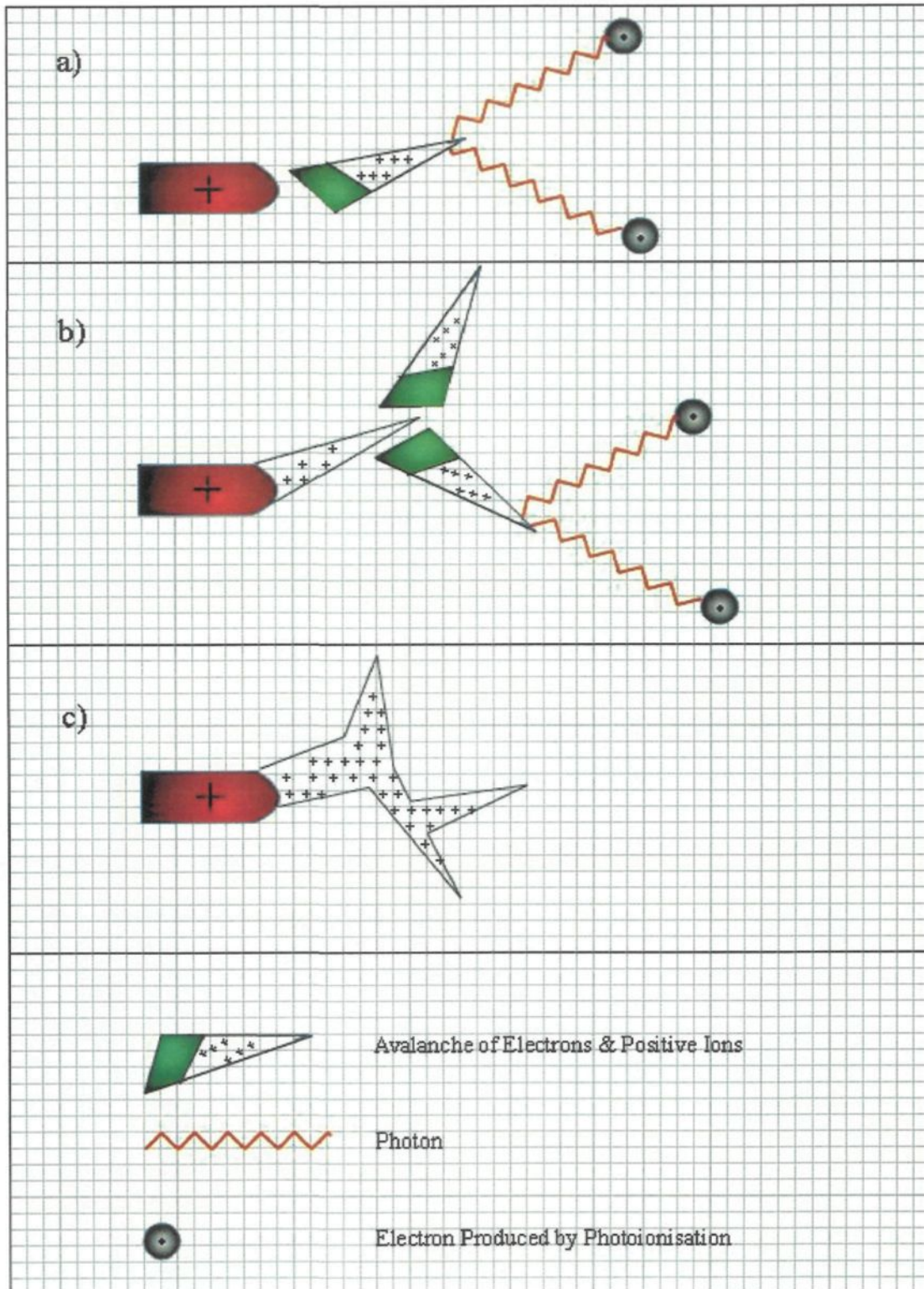
Figure 2-2: Schematic development of three modes of corona discharge at the anode

2.3.3 Corona Discharge in Alternating Current

In an alternating current, all of the discharge modes can occur. The produced space charges can modify the type or the intensity of the mode. The accumulation of the space charges depends on the frequency of the applied voltage and the distance between electrodes.

By a simple calculation [Nasser, 1971], it can be shown that the maximum distance between two parallel plane electrodes, d_{max} , necessary for the evacuation of the space charge in one alternation (before changing the polarity) equals to:

$$d_{max} = \frac{\mu \cdot E_{max}}{2\pi f}$$

Where:

f   Frequency of alternative field

μ   Mobility of ions

E_{max} Maximum amplitude of the electrical field

For a non-uniform field with coaxial configuration, the maximum distance equals to

$$(d_{max} + a)^2 - a^2 = a\mu E_o /f$$

a   Radius of central conductor

E_o Threshold field for corona effect

2.4. Electrical Wind

With a point-plane electrode configuration, ions of the same polarity are repelled from the highly stressed electrode [Loeb, 1965]. They gain momentum from the electrical field and as a consequence of the collisions, this momentum is passed on to the gas. This creates a pressure difference (an asymmetrical field corona discharge) in any section of the gas and produces a current of gas in motion, or an electrical wind. The existence of this wind has been known since the earliest electrostatic studies of the late 1600s. A sharp point yielding the current in the hundreds of microamperes from a good static generator will blow out a small candle flame from a distance of 1 cm [Loeb, 1965].

The gas velocities resulting from the wind are insignificant compared to the ionic drift velocities and are of no great consequence in the breakdown mechanism [Farzaneh, 1986]. Robinson formulated the following equation which relates the speed of the wind to the discharge current for one-dimensional electrical fields [Robinson, 1962]:

$$V = A \, (i_d \, / \, \rho_g \, \mu_m)^{1/2}$$

Where:

V Velocity of ionic wind

i_d Discharge current

ρ_g Volume mass of the gas between electrods

μ_m Mean mobility of ions

A Function coefficient of system geometry

2.5. Corona Discharge on Transmission Lines

The environment effects produced by corona discharges on conductors play an important role in the design and operation of high-voltage transmission lines. Radio interference and audible noise are the principal environmental consequences of corona on both AC and DC lines, while corona-generated space charge environment is also important in the case of DC lines. In foul weather, water drops hanging from transmission conductors cause an increase in corona activity and behave both as sources of various charge carriers, audible noise and electromagnetic interference and sinks of energy. In rainy weather, charge carriers from a transmission conductor to ground consist of molecular ions produced by corona discharge and water drops, which drip from the conductor or are charged on their way to ground. Loeb describes this phenomenon as follows: water drops falling in a uniform field becomes distorted and lowers the spark breakdown potential of the normal air. The induced positive end of these drops is drawn out to a fine point, which emits spray and a characteristic streamer like corona process. The induced negative ends shows some pointing but most of them are clearly defined and have a faint glow superficially resembling a negative point corona. That a negatively charged water surface should yield a negative point corona appears strange. Such Trichel pulse coronas in air require that the surface emit electrons by positive ion bombardment or else by photoelectric effect [Loeb L.B., 1963].

CHAPTER 3

REVIEW OF LITERATURE

3.1. INTRODUCTION

This chapter provides a survey of the previous research on corona discharge and its induced vibrations on the transmission lines. During the present research work, several papers and theses have been reviewed and analyzed (see References at pages 113~117). While it is not possible to review all of them in this chapter, some of the most important are reviewed.

We begin with M. Hara and his colleagues to introduce the modes of corona discharge and specific charge of water drops as well as formation of water drops in various electrical fields.

Then, the analytical model and numerical simulation method of Shah and Morgan is briefly discussed. To the best of my knowledge, they were the first group who developed a numerical model for vibrations induced by corona on transmission lines.

Experimental results presented by M. Farzaneh are a worthwhile thesaurus for researchers in this domain. Some of his results are reviewed in this chapter.

The research work of Maaroufi has been analyzed in the following of this chapter. Also the mathematical models of the applied forces on a water drop, suspended under a high voltage conductor are discussed.

A summary of P. Demers research work is the last part of this chapter. Methodology of his numerical simulation is explained and some drawbacks of his approaches are listed.

3.2. Hara M., Ishibe S., Akazaki M.

The main purpose of their research work [Hara & his colleagues, 1980,1981, 1979] is to show experimentally the relationship between the modes of corona discharge and the dripping manner of water drops from a high voltage conductor, as well as the threshold conditions.

They measured characteristics of the specific charge based on the polarity of the electrical field strength on the surface of an ACSR (Aluminum Conductor Steel Reinforced) conductor. Their results are shown in Figures 3-1 and 3-2.

These authors present four modes on the curve of the *specific charge of water drop* versus the *maximum field strength on a smooth inner conductor,* which explain the behavior of the water drops in the electrical field as follows:

Refering to Figures 3-3 and 3-4, mode I occurs at low field strength where the specific charge gradually increases with the field strength. Increasing the field strength beyond a certain value as point A, the specific charge suddenly decreases to some values which depends on the size of the inner conductor, and it recovers to the level of A. This region is termed mode II. As the field strength is further increased, a polarity effect appears. In fact, the value of the specific charge of water drops from a positive conductor indicates a sharp maximum value at point C in Figure 3-3.
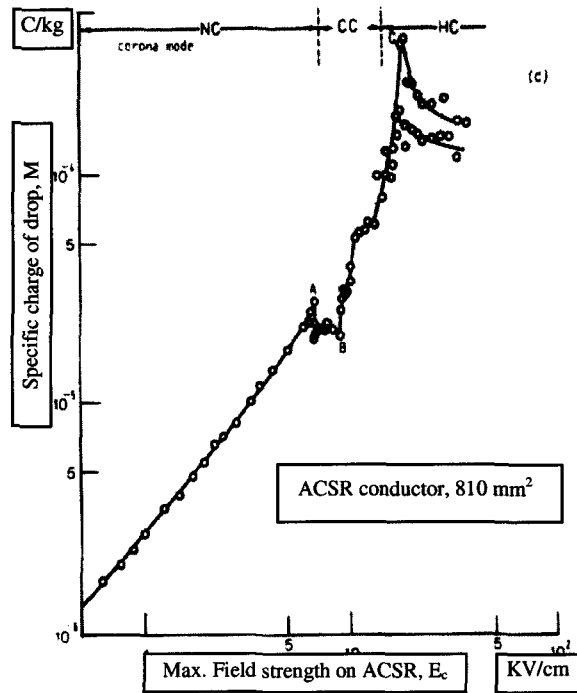
Figure 3-1: *Positive ACSR conductor*
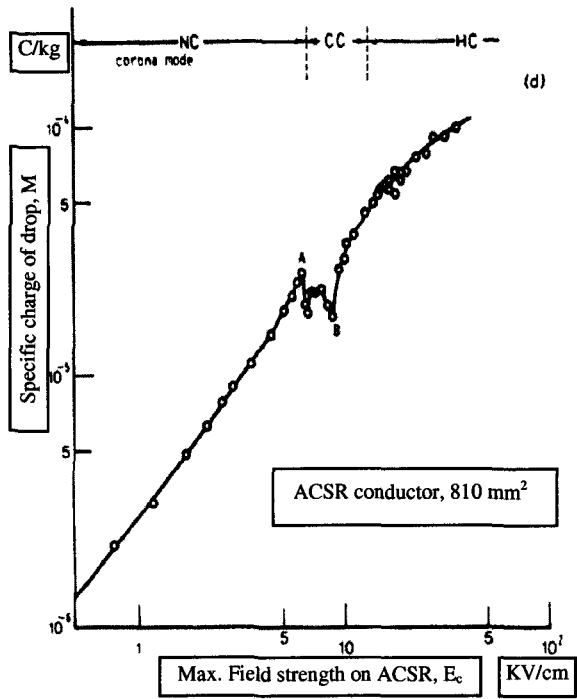
Figure 3-2: *Negative ACSR conductor*
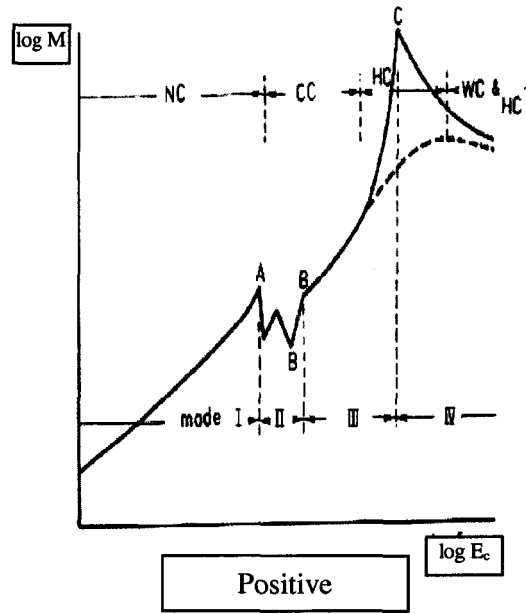
Figure 3-3: *Field strength on positive inner conductor, Ec*
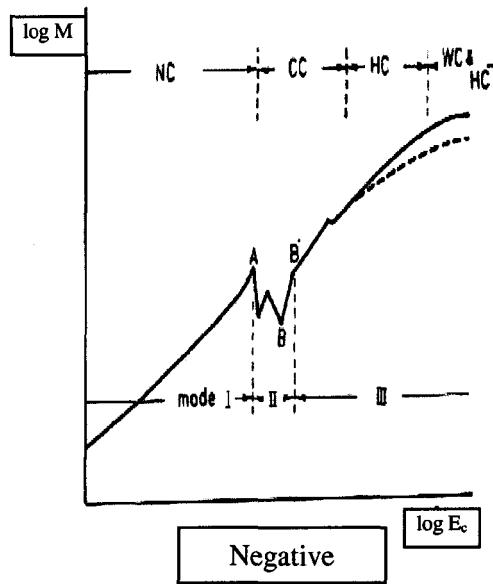
Figure 3-4: Field strength on negative inner conductor, Ec

25

This value depends on the inner conductor size and the flow rate of water supplied to the inner conductor. The region from the recovered point B' to the point C is defined as mode III, where the value of the specific charge increases with the field strength. The remaining region corresponding to higher field strengths is named mode IV.

In 1968, Akazaki M. and Lin S. defined two corona modes: "Crackling and Hissing Corona", for which the four modes of corona in this paper are an extension of the previous work [Akazaki M. and Lin S. ,1968]. As it is shown in Figures 3-1 to 3-4, the four modes can be also classified as: No-Corona (NC), Crackling Corona (CC), Hissing Corona (HC) and Wire Corona (WC).

The CC occurs at the moment of removal of water drops from the conductor or during a deformation of the suspended drop and produces the crackling sound. Continuously maintained corona accompanied by the continuous hissing sound appears on a water drop with a conical tip. This is termed Hissing Corona. The WC is corona discharge from the inner conductor and always accompanies the HC, and it also gives a hissing noise.

Hara M. and his colleagues [Hara, 1979] also illustrate the formation of water drops suspended on a conductor for different modes. Three samples of them are shown in Figures 3-5, 3-6, and 3-7. In addition, they measure the radius of the mother drops and their satellites for different field strength. They concluded that in the mode I, the mother drop radius is almost constant and is about three times or more of the corresponding satellites. In the mode II, the mother drops radius abruptly decreases. In mode III and IV with constant field strength, the drop radius for a positive conductor is smaller than for a negative conductor and has a sharp minimum at the field strength corresponding to the point C.
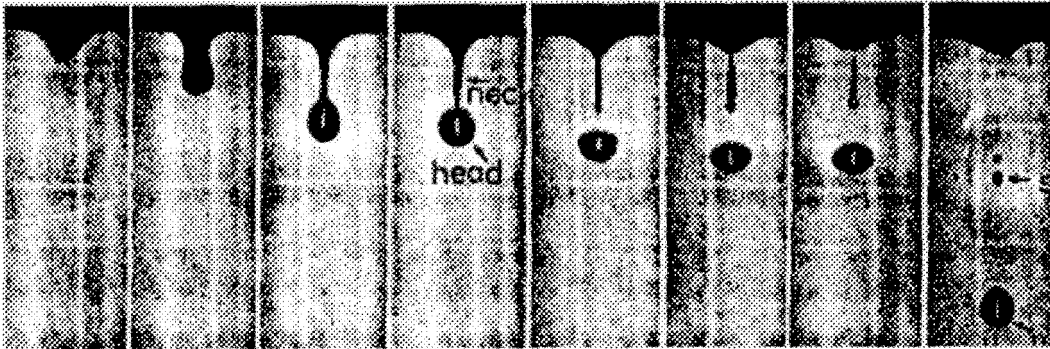
Figure 3-5: *Formation of water drop, Ec = 2 kV/cm, mode I*
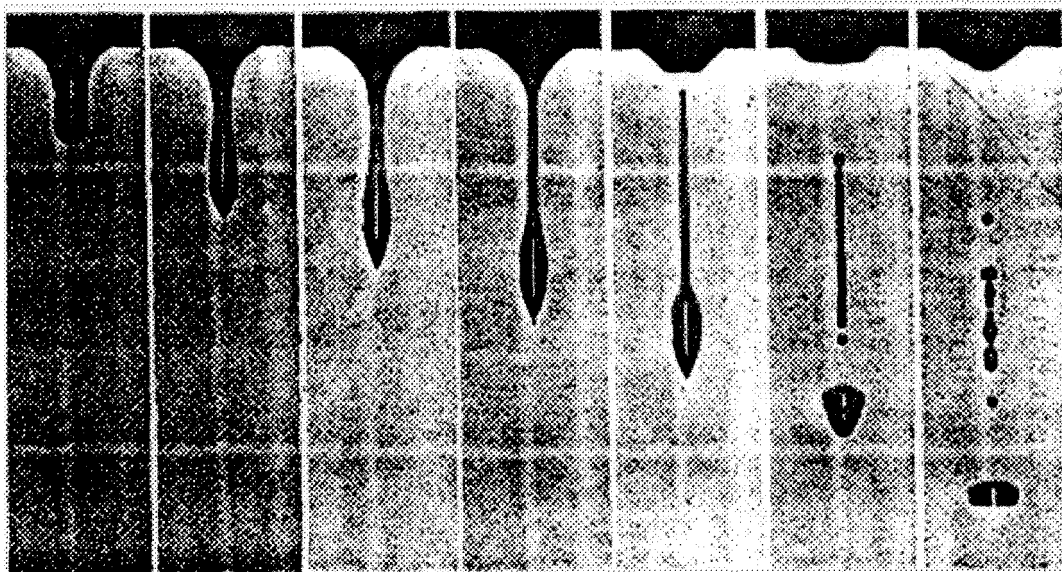
Figure 3-6: *Formation of water drop, Ec = 6.3 kV/cm, mode II*
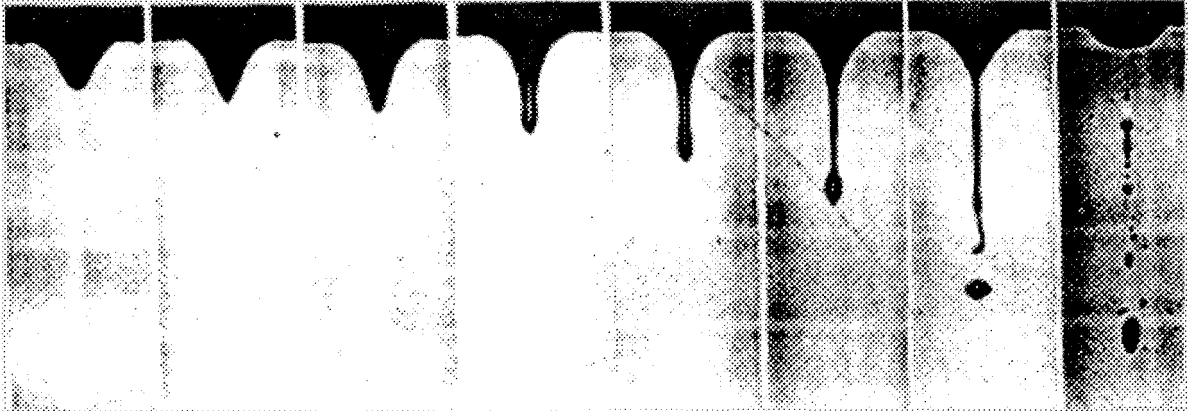
Figure 3-7: *Formation of water drop, Ec=10.1 kV/cm, at the starting point of the HC,*

mode III

3.3. Shah K. S., Morgan J. D.

According to my information, they were the first group who succeeded in doing a numerical simulation on the corona-induced vibration of high voltage transmission lines.

For numerical simulation, they apply some mathematical models [Shah, Morgan, 1976]. They use Hokierti J. calculations for the model of the electrical field at the water drop surface [Hokierti J., 1974] as follows:

$$E_T \approx \frac{3\left(\varepsilon_2 - \varepsilon_1\right)}{\varepsilon_2 + 2\varepsilon_1}\left|E_0\right|\cos\theta\,k$$

Where

ε_1 Relative dielectric constant of air

ε_2 Relative dielectric constant of water

E_0 Electrical field at the conductor surface

28

θ Angle made with the direction of the dipole moment

k Unit vector from center of the water drop to the point of calculation

The electrical force on a hemispherical water drop is calculated as:

$$F_{WD} = \frac{\varepsilon \pi}{4} \left[\frac{3(\varepsilon_2 - \varepsilon_1)}{2\varepsilon_1 + \varepsilon_2} \right]^2 |E_0|^2 a^2$$

Where

F_{WD} Total electric force in the downward direction

a Radius of the water drop in mm

For this analysis taking $\varepsilon_1 = 1.0$, $\varepsilon_2 = 80.0$ and $\varepsilon = 8.85 \times 10^{-12}$ Coulomb/Newton-meter^2 it is found that,

$$F_{WD} = 58.06 \times 10^{-18} E_0^2 a^2 \qquad \text{Newton}$$

The gravitational force on a water drop is calculated as:

Gravitational force = mass * acceleration due to gravity

Mass of a hemispherical drop = $\dfrac{1}{2} \dfrac{4}{3} \pi a^3 \times 10^{-6}$ kg   (a is in mm)

$$F_g = 20.546 \times 10^{-6} a^3 \qquad \text{Newton}$$

Shah and Morgan consider the sum of electrical and gravitational forces ($F_{WD} + F_g$), exerted on a water drop adhered to the conductor, as a downward force that acts on the conductor. They apply this force as an impulse force, that is one of the advantages of their work.

They use finite element methods to simulate numerically vibrations induced by corona on transmission lines. For the conductor oscillation analysis, the initial-boundary

value problem is formed using the wave equation. The impulse force is applied as an input force term and the solution is obtained for the non-homogeneous initial-boundary value problem. The solution is then modified to consider time and a random spatial distribution of forces.

They solve the problem for two cases of a transmission line with end supports at the same level and for different levels.

3.4. Masoud Farzaneh

M. Farzaneh follows the research work of Phan L. C. who was the founder of "Groupe de Recherche en Ingénierie de l'Environment Atmosphérique (GRIEA)" at the University of Quebec in Chicoutimi. Due to Farzaneh's research work, GRIEA has been known as the most important and significant laboratory in this domain in the world. He has worked on different aspects of physics of discharge. However, a comprehensive survey of all his works is not attempted to be presented here.

In his Ph.D. (Doctorat d'Etat) thesis [Farzaneh, 1986], he studied corona-induced vibration using experimental methods. In the first set-up, he places a single smooth hollow aluminum conductor on the axis of a cylindrical mesh cage and applies a high voltage to the conductor. Amplitude and the frequency of the vibrations (induced by corona) of this conductor under rain and for different polarities are one part of his results. He presents different experimental curves to illustrate the behavior of corona-induced vibration for various intensities of rain precipitation and in different polarities.

Variation of *amplitude of vibration* (induced by corona) versus *intensity of precipitation* is shown by three curves in Figure 3-8. Regarding these curves, the variation of amplitude is linear for different values of electrical field and for precipitation of rain less than 25 mm/h. For values bigger than 25 mm/h, the amplitude of vibrations becomes constant.
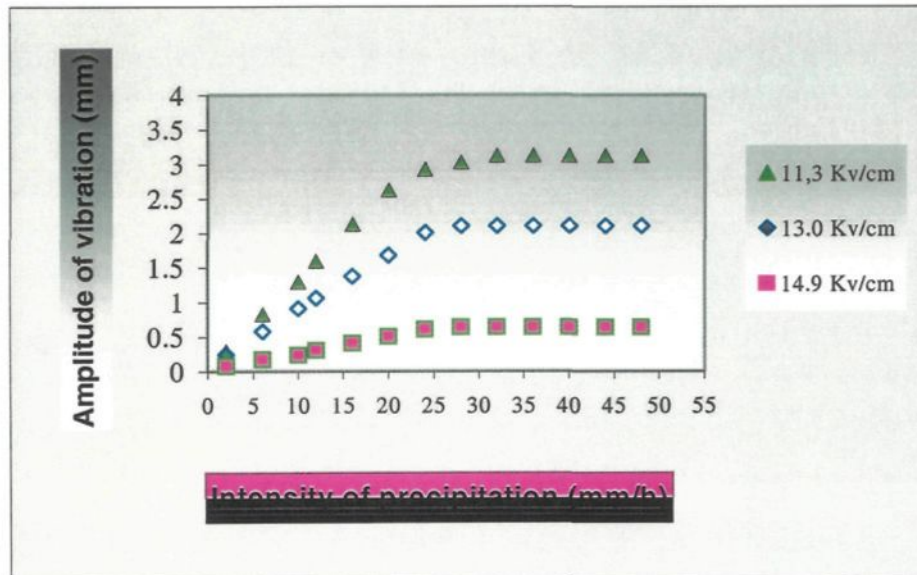
Figure 3-8: Amplitude of vibration versus intensity of precipitation

Then he presents a variation of *amplitude of vibration* (induced by corona) versus *electrical field on the surface of conducto*r. These experimental results for smooth and ACSR (Aluminum Conductor Steel Reinforced) conductors supplied with different polarities are illustrated in Figures 3-9 and 3-10.

On a smooth conductor (Figure 3-9), changes of amplitude is the same for DC positive and negative, and it is approximately linear for AC polarity.
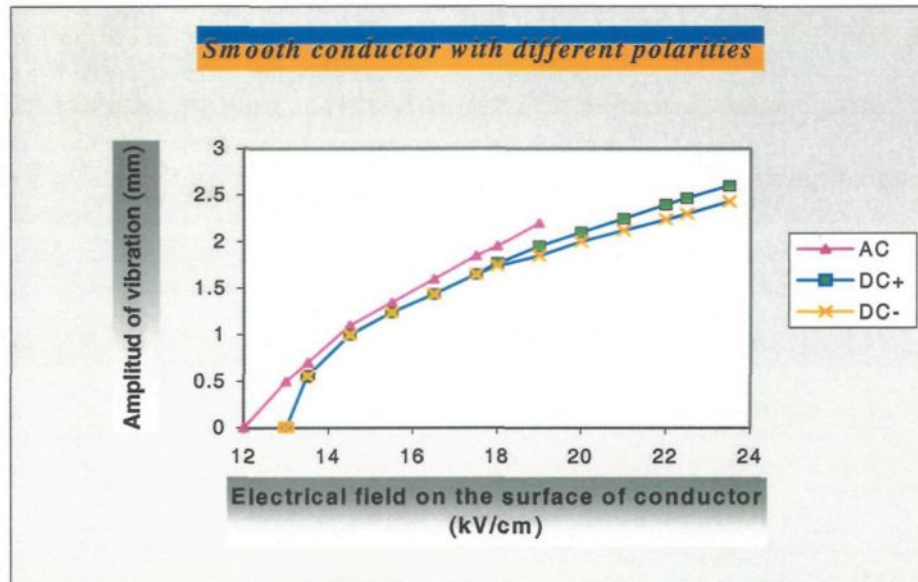
Figure 3-9: Amplitude of vibration versus electrical field, for different polarities

M. Farzaneh reported that on ACSR conductors, characteristic of the amplitude of vibration is completely different from smooth conductors. Interpretation of these results is given in Chapter 4.
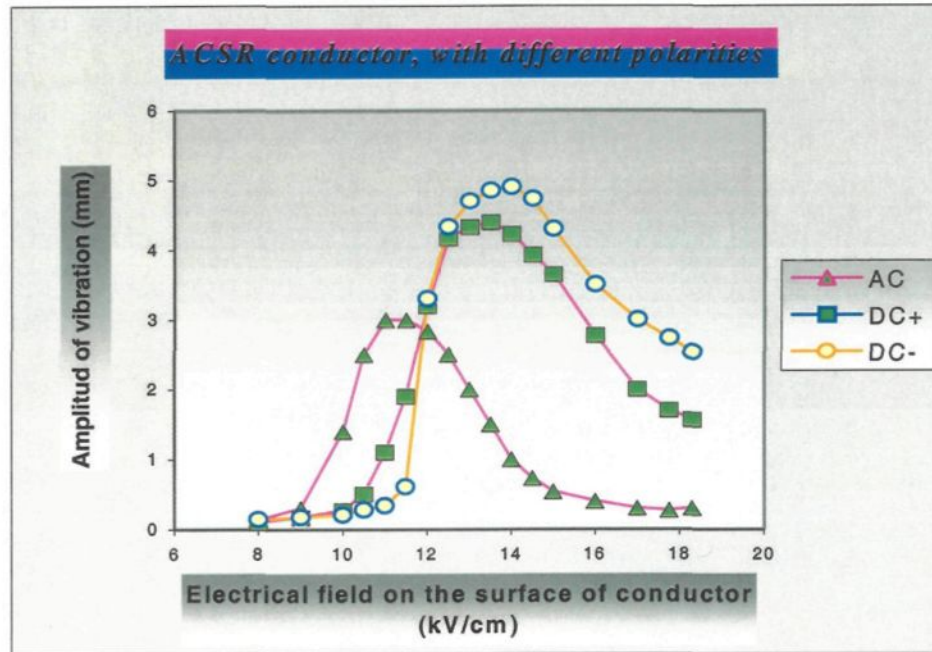
Figure 3-10: Amplitude of vibration versus electrical field, for different polarities

He also submits the value of discharge current for different electrical fields and different polarities.

Then he replaces hanging water drops on the smooth conductor by conical metal points and measures the amplitude of vibrations and corona current as a function of the number of the metal points and estimates the corona-induced force as approximately 10^{-3} Newton/drop.[Farzaneh, 1986, pp. 129].

For comparing the effect of ionic wind with corona space charge, he presents an experimental set-up, which is a pinwheel consisting of a rotating arm at the ends with two conical points fixed on opposing sides [Farzaneh, 1986, pp. 131]. The exerted forces on these two conical points are determined from the acceleration of the arm when subjected to a high voltage. By this method, he was able to measure the velocity of the ionic wind in the

vicinity of water drop, and to estimate the amplitude of the reactive force due to the ionic wind.

By other experimental set-ups, he observes that even in absence of the ionic wind, a high voltage sphere suspended above a grounded plane vibrates when an intermittent space charge is injected in the intervening space [Farzaneh, 1986, pp. 175].

3.5. Maaroufi Mohamed

Maaroufi presents an analytical method for calculation of the amplitude of the vibrations induced by corona on transmission lines [Maaroufi, 1989].

Maaroufi employs the same experimental model as Farzaneh M. used in his laboratory. His analytical model is also based on the experimental results which Prof. Farzaneh found out [Farzaneh M.,1986].

From literature, he has chosen the better forms for the forces, which are applied to the suspended water drops under a high voltage conductor. The origin of the applied forces is presented as [Maaroufi M.,1989, pp. 67] :

- Reaction force due to the ejection of water drops;

  The ejection of the water drop can happen when the resultant of following forces is unbalanced.

- Weight of suspended water drop;

- Electrostatic force which lead to an elongation of water drop;

- Inertia force due to the movement of conductor;

The value of the reaction force is given as:

$$F_r = \frac{2}{3} \rho \, \pi a^3$$

Where

F_r Reaction force

a   Radius of water drop

ρ Specific weight of water

• Repulsion force between the ejected droplets and the high voltage conductor;

The nature of this repulsion force is electrostatic. Maaroufi introduces this force as Shah K. S. does in his research work [Shah K. S. , Morgan J. D., 1976] :

$$F_{re} = \frac{9\pi \, \varepsilon_0}{4} a^2 E_0^2$$

Where

F_{re} Repulsion force

ε_0 Dielectric constant of vacuum

a Average radius of water drop

E_0 Superficial electrical field on the conductor

• Force due to the electrical wind;

As Farzaneh shows in his research work, contribution of the force due to the electrical wind is less than 20% of the total force acting on the conductor. It is about 3×10^{-4} N/drop[Farzaneh M., 1986].

35

- Force due to the space charges ;

Considering a point charge $+q$ located in the center of a conductor, at a distance h from the ground. If a space charge $+q'$, is located at a distance r from the center of the conductor, the produced force by space charge is expressed by:

$$F = K\left(\frac{qq'}{r} - \frac{qq'}{2h-r} - \frac{q^2}{2h} \right)$$

He also investigates the influence of humidity, fog, and melted snow on the high voltage conductor.

3.6. Demers, Pierre

He simulates the vibrations induced by the corona of high voltage transmission lines [Demers, 1994]. His numerical simulation is based on finite element methods. He chooses modal superposition techniques which transfer basic differential equations to a system of independent equations, while each equation represents one mode of vibrations. Discretisation of time is realized by using the finite difference method.

At the beginning, he works on the smooth conductor, which is explained in Farzaneh's research work. He simulates vibrations of this high voltage conductor under artificial rain. He analyses that each ejection of water droplets applies an upward force on the conductor. The value of this force is also calculated by Farzaneh [Farzaneh M. ,1986]. Demers follows two theories to formulate this force. In the first theory, all of the inputs, like the distribution of the water drops on the conductor, and the moment of ejection of the

drops, are calculated statistically. In the second theory, the balance of four forces

determine the moment of ejection of water drop. These forces are given as:

- force due to the weight and inertia of water drop;

$$F_{po} = \rho_{water} \, V \, a_{cc} + \rho_{water} \, V \, g$$

- vertical component of the electrostatic force;[Shah K. S., Morgan J. D., 1976]

$$Fy_{wd} = 58.06 \times 10^{-18} E_0^{\,2} \, r_{drop}^2$$

- force due to the superficial tension;

$$F_{ten} = 2 \, \pi \, r_{drop} \gamma_{water}$$

- force induced by corona effect;[Farzaneh M. 1986]

$$F_{ind} = 0.0005 \quad N/drop$$

Where

V Volume of water drop at each time step

a_{cc} Acceleration of water drop at each time step

E_0 Electrical field on the conductor surface

r_{drop} Radius of water drop at each time step

γ_{water} Tension of the surface (N/m^2)

Finally, he decides to choose the second theory, which involves balance of forces.

To apply inputs to the simulation program, he uses the experimental results which

were obtained by Farzaneh [Farzaneh M. ,1986]. In spite of the great research that Demers

has done he employs some of the inputs incorrectly. For example, in the force balance

method, the force induced by corona is considered as a constant, while it is supposed to be considered as an impulse force. Also, the moment of application of this force is developed with a 10 ms delay after ejection of water droplet. He applies this delay, because in the experimental model that Farzaneh M. has developed, there is a distance between conductor and grounded cage. This distance causes 10 ms difference between the time of separation of the water droplets from the conductor. To simulate the discharge current, this time delay should be considered, because in this model, the sensor of the discharge current is placed on the cage and it can sense the ejection of droplets 10 millisecond after its separation from the conductor. Therefore, the delay should be used in the simulation of the discharge current and it should not be considered in the force calculation.

To obtain the amplitude of vibrations identical to the value that Farzaneh reported, Demers employs a coefficient K . This coefficient is a ratio between total volume of water drop and the residual volume of water drop (after ejection of droplet), which Demers found out with trial and error in his simulation program.

He finally repeats this simulation for a specific transmission line.

CHAPTER 4

EXPERIMENTAL SIMULATION

4.1. INTRODUCTION

Since the advent of high voltage transmission, much attention has been directed towards the study and control of corona. Under wet condition, occurrence of corona on high voltage transmission lines causes corona-induced vibration. This kind of vibration of transmission line is generally observed under rainfall and in the presence of high electrical field strength at the surface of the conductors. The appearance of this vibration will be eliminated by wind strong enough to remove the majority of the suspended water drops on the transmission line [Shah, Morgan, 1976].

Several experiences are performed by different researchers to investigate this phenomenon. In most experimental set-ups, a short conductor subjected to the high voltage is placed in the middle of a grounded cage. To provide a wet condition, water drops are produced by an artificial rain [Farzaneh M., 1986] or by applying a single water drop on the middle of the conductor [Hamal M., 1991]. Even in an experimental model, conical aluminum points are placed under a high voltage conductor to simulate the static situation of the water drops on a high voltage conductor [Farzaneh M., 1984].

4.2. Experimental Model

The experimental model, which is used in this research, helps to explore the characteristics of the vibration of transmission lines induced by the corona effect. This

model provides a facility to investigate the influence of different factors on the vibration of high voltage conductors under rain. Control of the rain precipitation and adjustment of the value and the polarity of the high voltage supply is the most significant feature of this model.

This experimental model is placed in the Physic of Discharge Laboratory of GRIEA (Groupe de Recherche en Ingénierie de l'Environnement Atmosphérique) at the University of Quebec in Chicoutimi. Since this model has been installed at UQAC, several students have been studied different aspects of the physics of discharge, and of various parameters on the vibration of transmission lines induced by corona.

The following sections describe the assembly of the experimental model:

4.2.1 Schematic

The model consists of a short conductor, along the axis of a cylindrical mesh cage. The cage has three parts isolated from each other and connected to the ground. A high voltage circuit that is explained in the next section supplies the short conductor. To produce water drops on the conductor, a system of twelve nozzles is installed over the cage. The water is controlled by a valve and measured by a flow meter that comes through the nozzles and is sprayed on the conductor.

In Figure 4-1, a schematic of the experimental assembly is shown. A short hollow smooth aluminum conductor, 4.0 m in length and 3.2 cm in diameter (thickness 0.2 cm), is placed along the axis of the cage. The cage has an interior diameter of 1 m and the central

part of cage has a 2.0 m length while the two end sections have a length of 0.3 m. Two insulators with a height of 1.0 m support two ends of the conductor. Artificial rain is produced by a system of twelve nozzles, Wagner no.5, placed at an angle of 30° to the vertical plane containing the axis of the conductor.
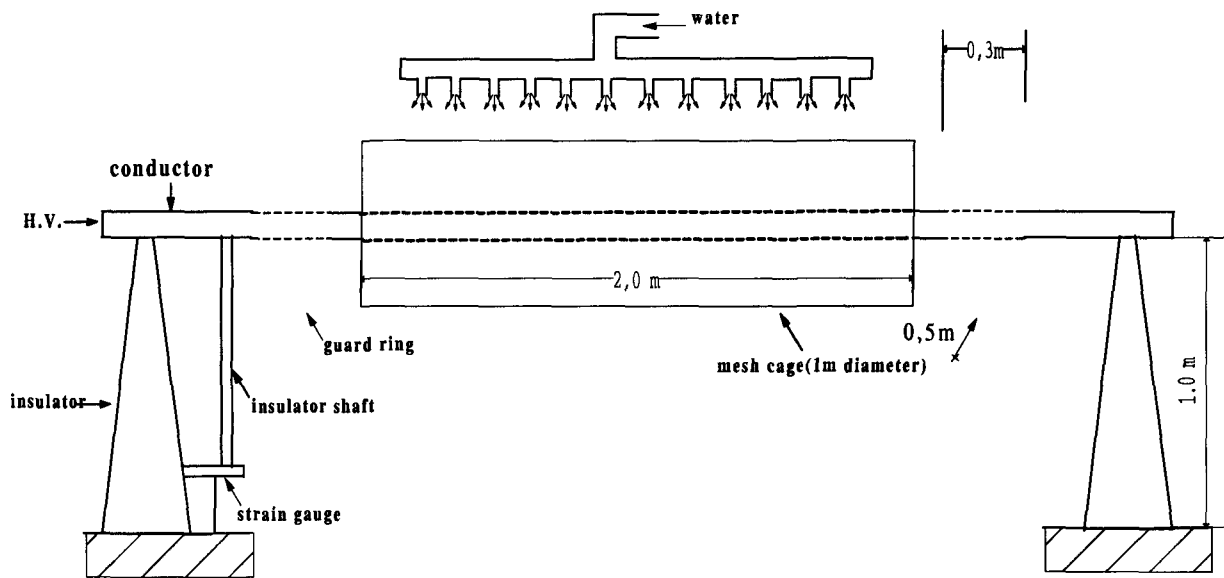
Figure 4-1: *Schematic of the experimental assembly with a smooth conductor*
[Farzaneh, 1984]

For the experimental simulation, two set-ups are performed. In the first set-up, a smooth hollow aluminum conductor is placed along the axis of the mesh cage. In the second one an ACSR (Aluminum Conductor Steel Reinforced) conductor is considered to simulate a section of transmission lines conductors. The following set-up shows the first set-up for the short smooth conductor.
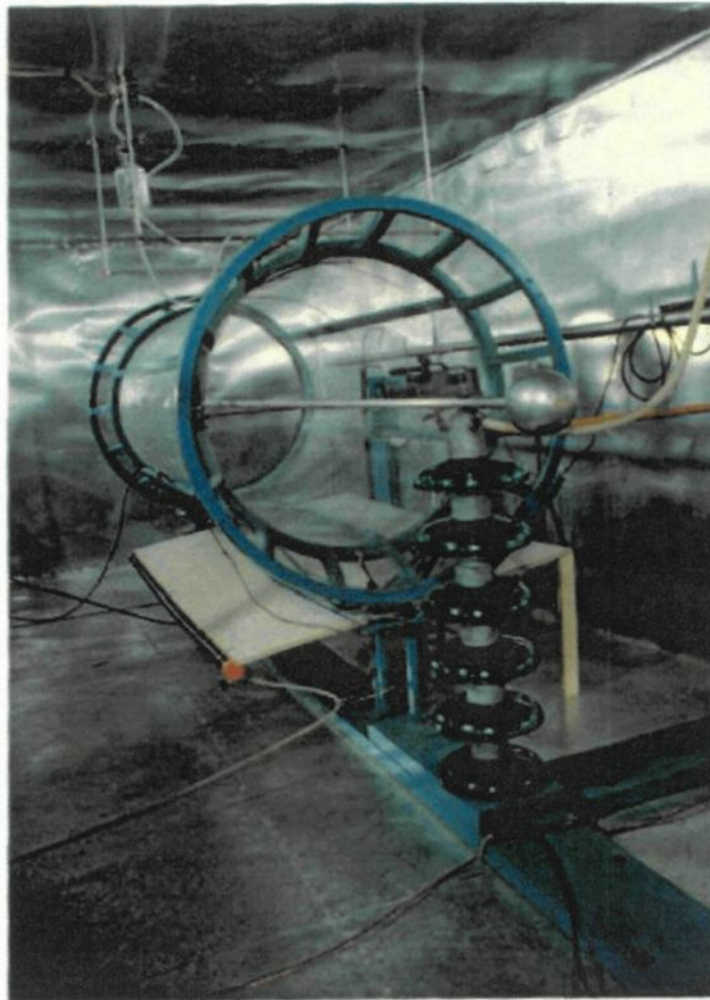
Figure 4-2: *First set-up, hollow smooth conductor* [Farzaneh, 1984]

On the first experimental model (first set-up), the natural frequencies and amplitudes of the vibrations (induced by corona) are measured. These measurements are repeated for different polarities and values of the electrical field supplied to the conductor. The shape of the water drops suspended under the high voltage conductor and the forces applied to the drops are the most important part of the results in this phase.

On the second experimental model (second set-up), the approach of complementary model is followed. To achieve more precision, an ACSR (Aluminum Conductor Steel Reinforced) conductor replaces the hollow smooth conductor. Since this conductor consisted of twisted strands, the manner of flow of the artificial rain on the surface of the conductor and the formation of water drops suspended to the conductor are more similar to the fact on the transmission lines.

4.2.2   High voltage Circuits

The high voltage section has two transformers, which are isolated with oil. A maximum voltage of 100 kV or 200 kV can be provided with one or two stages of the transformers. The output voltage of the transformers is applied to a component of resistors, capacitors and diodes to obtain an adequate type and polarity of voltage.

In the following table (Table 4-1), the component features of the high voltage assembly are given:

SYMBOL	ELEMENT	FEATURES
TEO 100/10	Transformer 100 kV	ratio : 2x220 V/ 100 kV /220V 5 kVA short circuit tension : 5%
TEOK 200/10	Cascade Transformer	ratio : 2x220 V/ 100-200 kV 5 kVA short circuit tension : 5-7%
GS	Selenium Diode	500 kΩ protection resistance, 5 mA max. inverse tension : 140 kV
CM	Measurement Capacitor	100 pF , 140 kV
CS	Impulse Capacitor	6000 pF , 140 kV
RM	Measurement Resistance	140 MΩ , 140 kV , 1 mA
RL	Load Resistance	50 MΩ ,140 kV

Table 4-1: Component features of the high voltage assembly

The assembly of the high voltage apparatus is a modular system from Messwandler-Bau Company. The different elements, described in the above Table, have the standard dimensions and are easy to fix. This set of elements gives a possibility to provide different types and polarities of the voltage as DC positive, DC negative, alternative and even impulse voltage. A two-stages transformer can provide two more times the maximum voltage.

The nominal values of the high voltage module for different natures of the voltage are as follows (Table 4-2):

NATURE OF VOLTAGE	ONE STAGE	TWO STAGE (CASCADE)
Alternative	100 kV 5 kVA	200 kV 5 KVA
Continuous	100 kV 5 mA	200 kV 5 mA
Impulse (1.5 x 50µs)	130 kV 85 W	260 kV 170 W

Table 4-2: Normal values of the high voltage module

Different types of voltage are applied to these experimental set-ups. The applied circuits for AC and DC voltages are as follows:
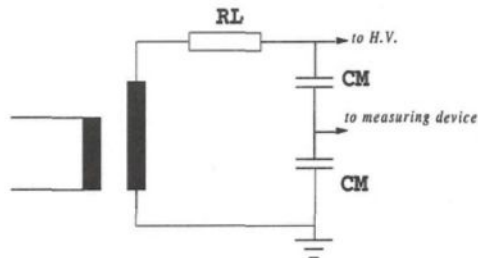
Figure 4-3: *Alternative Voltage, 100 kV, 5 mA*
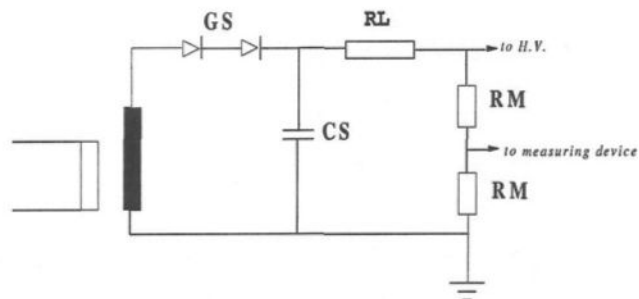
Figure 4-4: *DC Voltage, 100 kV, 5 mA*

The two next photos (Figure 4-5, Figure 4-6) show the assembly of the high voltage and the method of one or two stages circuit. The facility for providing the adequate circuit is a feature for this system.
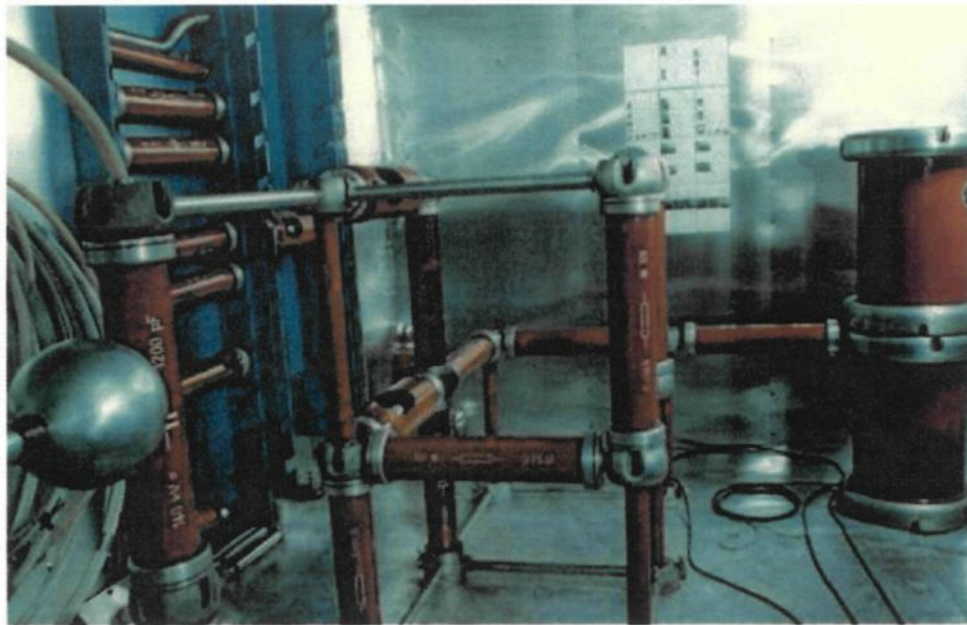
Figure 4-5: *Two-stages assembly for DC voltage*

Figure 4-6: *One-stage assembly for DC voltage*

A control desk (Figure 4-7) controls all the functions of the high voltage assembly. The most important part of this desk is a mono phase transformer, 5 kVA / 0~230 V, which supplies the high voltage transformer. The value of the high voltage is controllable by adjusting the output voltage of this transformer.

Supply 220 V / 50 Hz

Primary Contactor

6 A

V

Push Bottom with key

Tuning Transformer
5 kVA / 0-230 V

Isolation Transformer
220 / 220 V 0.5 kVA

V

A

Voltage of Control Desk

Secondary Contactor

towards H.V. Transformer
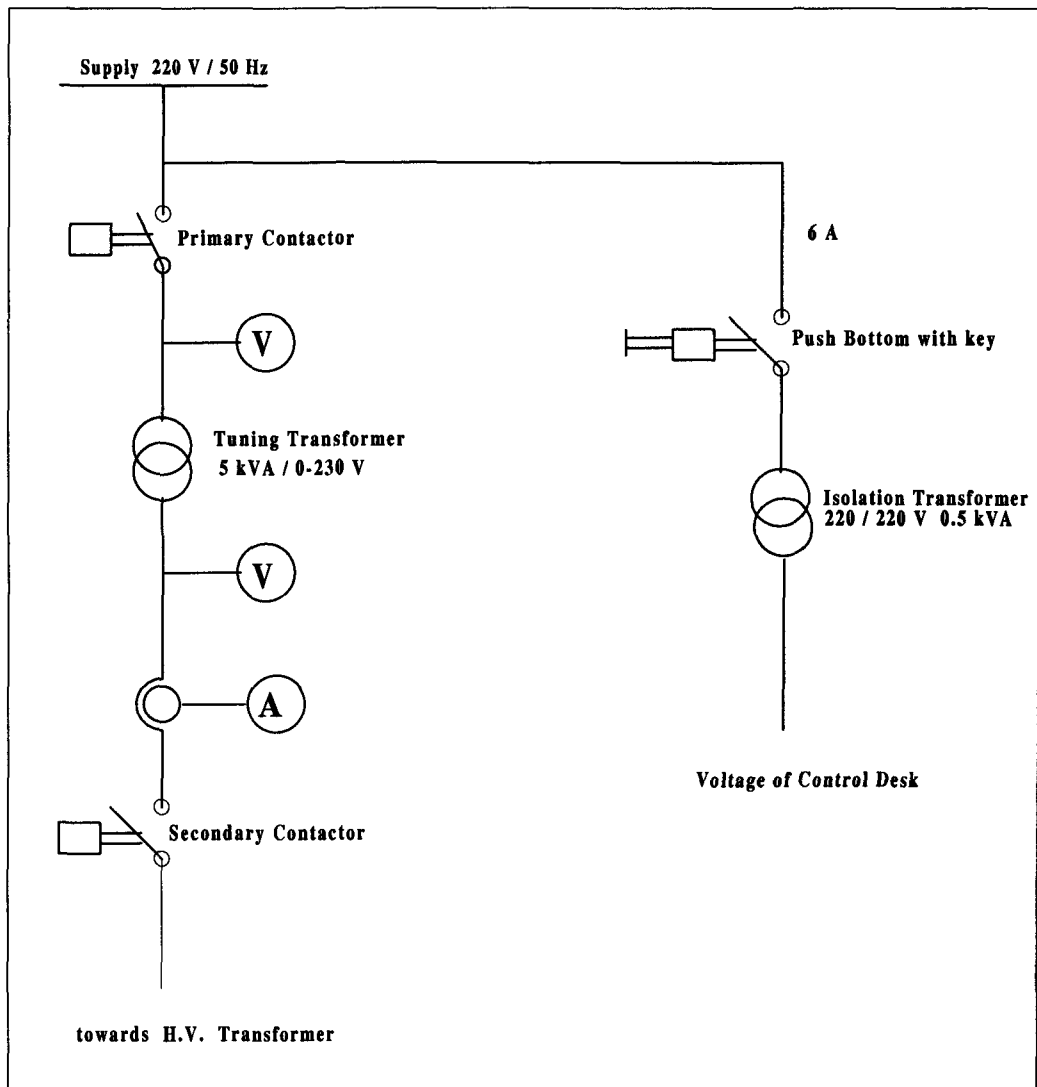
Figure 4-7: *Schematic of the control desk*

4.2.3 Flow meter

One flow meter is used for measuring the flow of sprayed water by the twelve nozzles. The flow meter has a small valve that precisely adjusts the volume of passing water per second. It is from Lab Crest Div. F.&P. Company and its features are noted as :

- meter tube, Cat No. 448-324

- float material : stainless steel

- float diameter : 1/4 inch

The working curve of this flow meter is as follows (Figure 4-8):

Conversion curve of flow meter
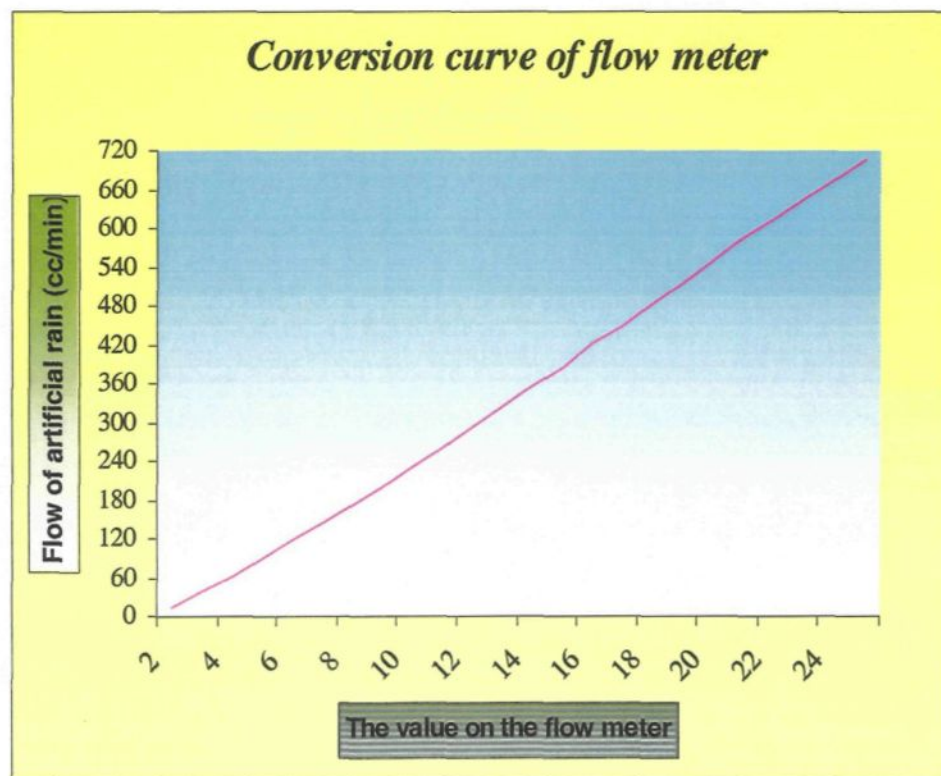
Figure 4-8: *Conversion curve of the Flow meter*

4.2.4 Motion Analyzer

The KODAK EKTAPRO EM Motion Analyzer is an instrument kit from the Optikon Corp. Ltd., which makes possible the study of the phenomena that happen in a short period. The menu driven keypad, interactive displays and helpful image capturing techniques help to analyze the problem with more facility. The live setup feature allows the user to be sure that the image is exactly what it is required and the image on the video monitor is what will be captured in memory when the RECORD key is pressed. The recorded images are immediately available for analysis.

The assembly of the Motion Analyzer consists of three parts as they are shown in Fig. 4-9:

1) *Kodak Ektapro Imager*

It is an advanced camera with remote control. The features of the imager are mentioned in Figure 4-10.

2) *Kodak Ektapro EM Processor*

A processor analyzes the image taken by the high-speed camera (imager) and sends the information to a visual system as a set of VCR and TV. It records at 50, 125, 250, 500, 1000, 2000, 3000, 4000, 6000, and 12000 pictures per second. There is a possibility to select the grey scale resolution between 256 (default value), 128, 64, 32, 16, 8 and 4 levels. As the number of gray level is decreased, the record time is increased. Also, Recticle option provides a facility to measure distance between two points. The measured distance is in pixels and to change it into the metric system, it is necessary to know the changing ratio in each adjustment of the camera.

KODAK EKTAPRO
EM Processor

KEYPAD
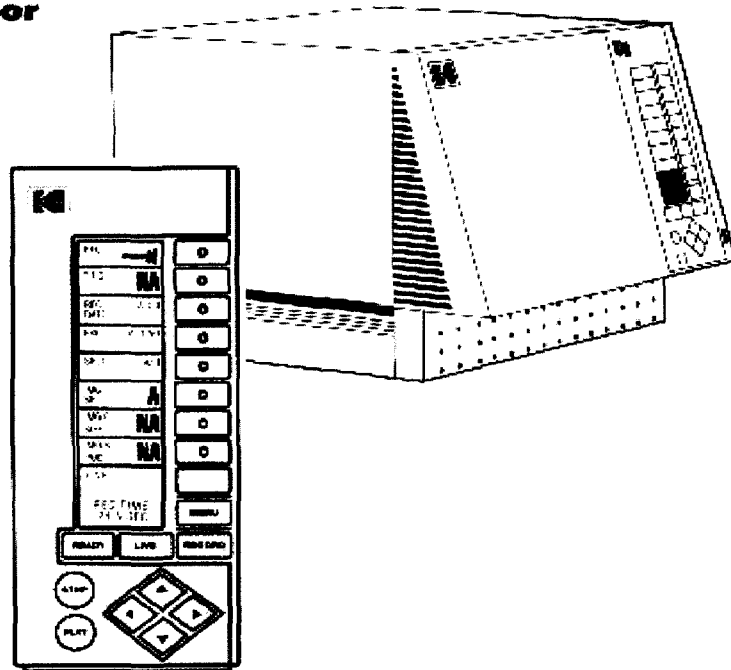
KODAK EKTAPRO
Imager
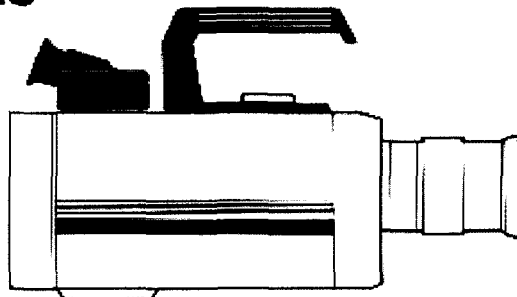
Figure 4-9: *KODAK EKTAPRO EM Motion Analyzer*
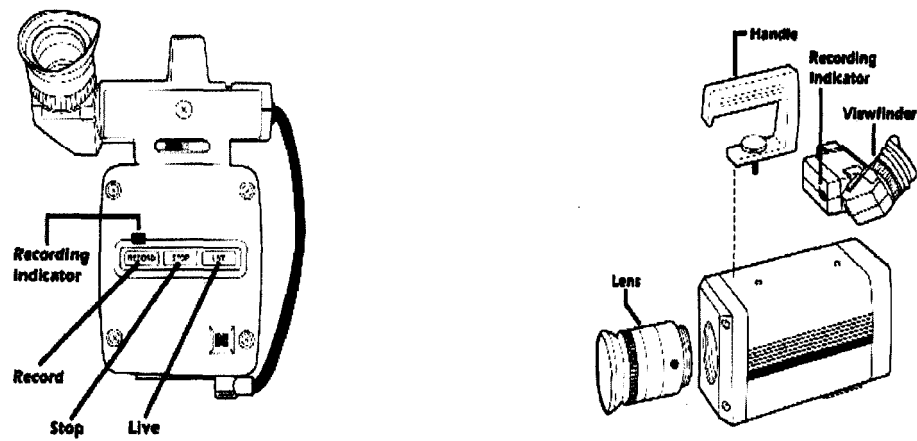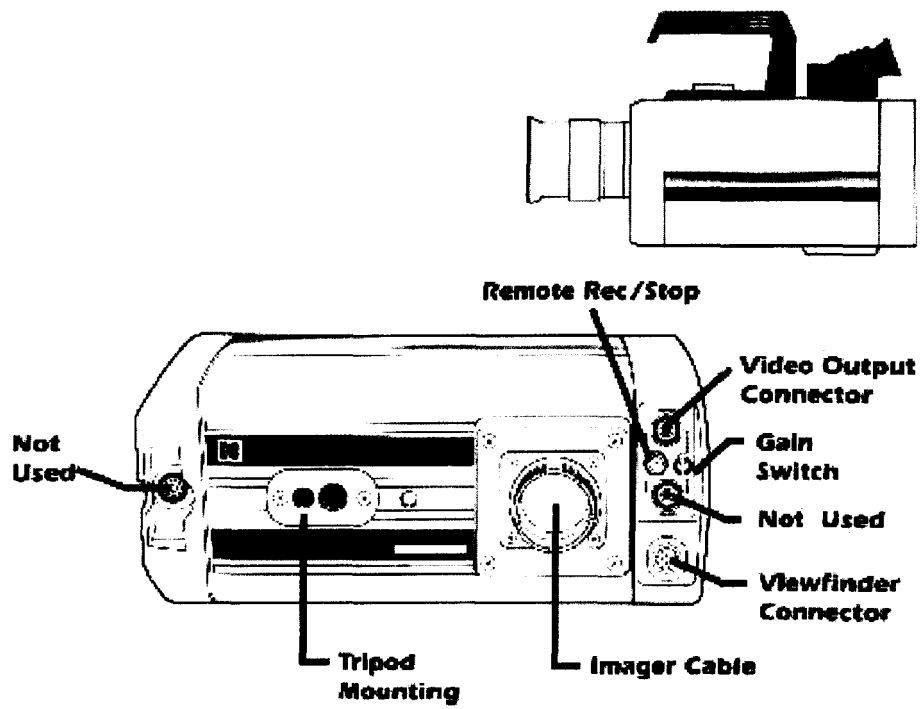
Figure 4-10: *Features of KODAK EKTAPRO Imager*

3) *Keypad*

The keypad controls all the motion analyzer functions and provides status information. As it is shown in Figure 4-9, it has several control keys and a large liquid crystal display (LCD).

4.2.5   Digitizing Oscilloscope

The HP 54111D is a fully programmable real time digitizing oscilloscope from the Hewlett-Packard Company. It uses a sample rate of 1 GS/second, which gives a repetitive bandwidth of 500 MHz, and a single shot bandwidth of 250 MHz. The inputs include two vertical signal channels and two trigger channels.

Information for operating, programming and interfacing the HP 54111D is contained in the manuals supplied with the instrument.

4.3. Drop Profile

From the review of the previous research works, it is obvious that the shape of the suspended drops under a high voltage conductor is related to the applied voltage and precipitation of rainfall. To search more about this relation and to acquire enough information for the numerical simulation, we decided to present a drop profile. To achieve this, the experimental model and the high-speed camera described in the previous section are the best tools. As it was mentioned in the characteristics of high-speed camera, taking 12000 images per second and the possibility of image record of this camera helped to represent a precise profile of water drops (refer to Appendix).

To explain the behavior of suspended water drops under a high voltage conductor, we start with a conductor under rainfall and in the absence of high voltage.
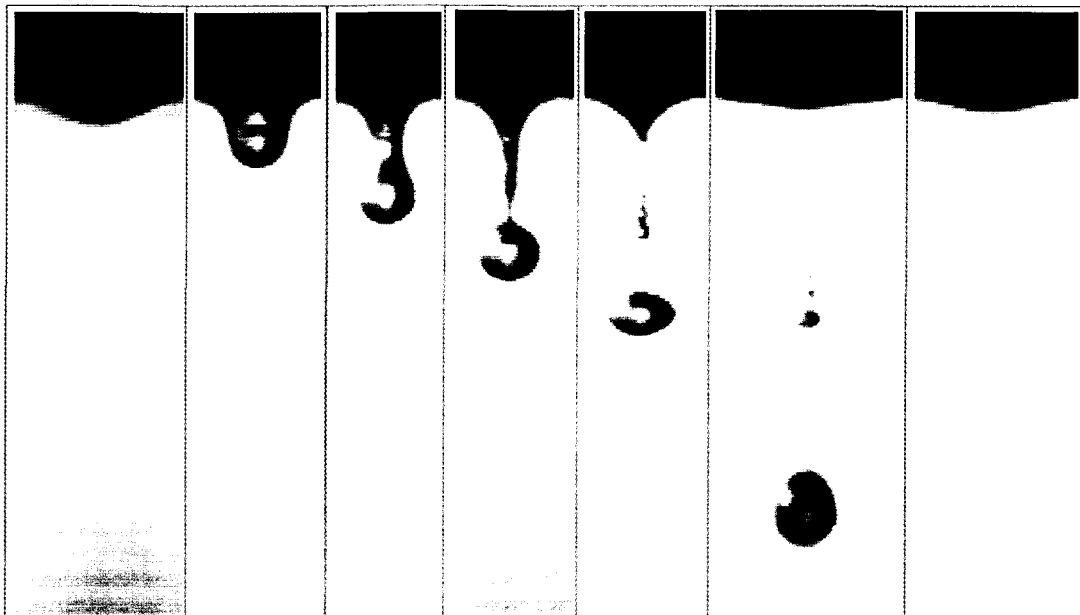
Figure 4-11: *Smooth conductor, without tension (6000 images per second)*

As it shown in Figure 4-11, accumulation of water under the conductor produces the hemispherical drop. Different forces act on the suspended water drops and bring out changes to the shape of drop. Gravity, surface tension and adhesive forces are involved in elongation of a drop and consequently in ejection of its water droplet. Ejected droplet has a portion of the total amount of the drop volume, which is the subject of the next section.

When a droplet ejects from its drop, the balance result of the mentioned forces is towards the earth. Because of the reaction force, there is an upward force with the same values that cause the residual volume of water to stick on the conductor after the ejection. Encore, with accumulation of water under the conductor, this cycle repeats again.

The following forces participate in the force balance equation of a suspended water drop suspended under the high voltage conductor:

- Inertia force

- Gravity force

- Electrostatic force

- Surface tension

- Corona-Induced force

These forces are explained in details in chapter five.

Referring to the Figures in the Appendix (Figures A-1 to A-6) for the drop profile of an ACSR conductor, it is shown that by applying a high voltage to the conductor, the shapes of drops are no longer hemispherical. In most of the experimental results, drops keep conic shape except for a very high voltage and or heavy precipitation. The results for smooth conductors are the same as for ACSR conductors. However, smooth conductors

have a more synchronize profile. It means that, due to the shape and torsion of the ACSR

conductors for lower voltage and precipitation, drops want to follow the conductor shape

and this brings out more disturbances. But for higher voltages and more precipitation of

rain with larger amplitude of vibration, the shape of the conductor can not affect the results.

In Figure 4-12, the drop profile of a smooth conductor under a positive DC voltage of 50

kV, and an artificial rain with 90 CC/min flow, is shown. On this profile, the formation of

the drop to a conic shape and then the elongation of the drop, which leads to the ejection of

droplet, are shown up. As it is mentioned in chapter 5, the forces acting on the water drops

cause a sinusoidal motion for the conductor. At the upward movement of the conductor, the

residual volume of the ejected drop flattens on the surface of the conductor.
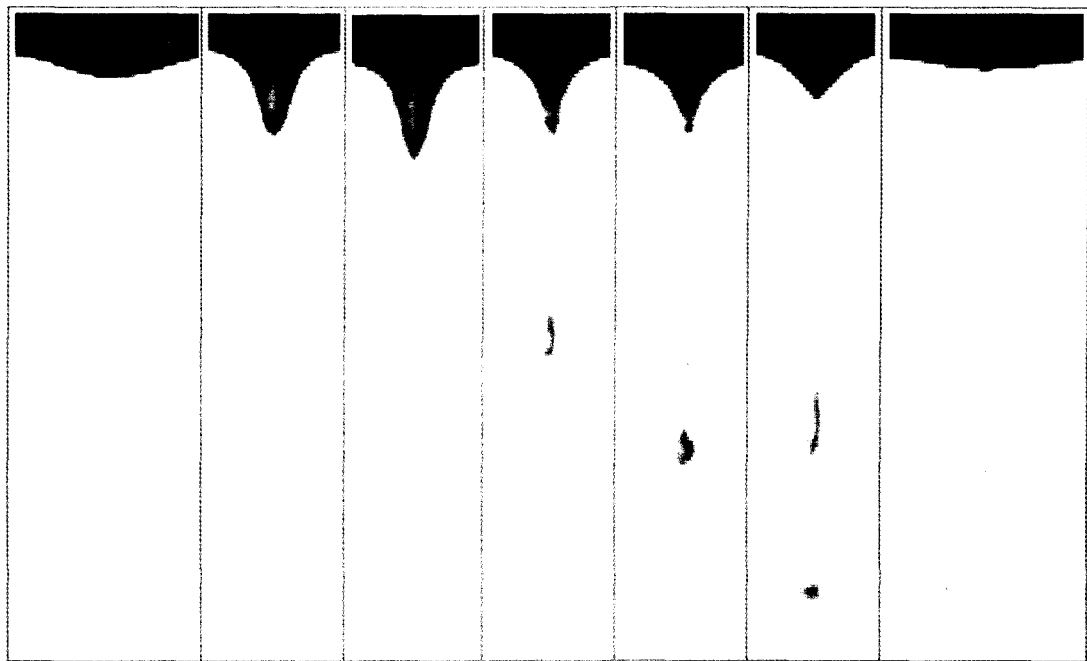
Figure 4-12: *Smooth conductor, DC+, flow=80CC/min, electrical field=50kV*
(12000 images per second)

To investigate the shape of drops and their droplets, experimental results for the ACSR conductor, in different polarities and intensities and under various precipitation of rain are illustrated in the Appendix. It is shown that as far as the applied high voltage increases, the drop shape becomes more conic and the elongation of drops occurs faster, which lead to an earlier ejection. As it is mentioned, each drop ejection applies an upward reaction force that leads to the vibration of the high voltage conductor. Therefore, it is mostly the increase in the number of drop ejection that increases the amplitude of vibration.

The same scenario takes place when the precipitation of rain on a high voltage conductor increases. This means that, the augmentation of the rain intensity accumulates the essential volume of water for ejection in a shorter period of time and creates a higher amplitude of vibration.

In most cases, the increase of both parameters, the high voltage and the precipitation of rain, applies as a consequence larger amplitude of vibration.

4.4. Variations of Drops Volume

As it can be interpreted from the drop profile (refer to the Appendix), the volume of a suspended water drop under a high voltage conductor is a time variable. When a drop enlarges, depending on the electrical field strength at the surface of conductor and the precipitation of rain, it will be ejected at a certain level of elongation. The event of ejection cannot separate the whole volume of the suspended water drop from the conductor. The rest volume of a suspended water drop after ejection is named residual.

To achieve a successful numerical simulation, the volume of the drop just before ejection and its residual are required (refer to Chapter 5). Two following sections illustrate these parameters for the both kind of conductors, ACSR and smooth.

4.4.1   Volume of water drops on the Smooth Conductor

A significant result of this group of experiments is about the fact that the characteristic of the drop volume is not related to the strength of the electrical field. But the variation of this parameter with respect to the intensity of precipitation changes for three different voltage polarities.

Figure 4-13 illustrates the volume of water drops just before ejection from an experimental hollow smooth conductor.

The experimental results show that for DC+ and DC-, the variation of this volume versus the intensity of the artificial rain is linear until the intensity of rain reaches to about 20 mm/h. Then the volume of the suspended drop just before ejection is fixed and the increase on the flow of rain does not affect that anymore.

This kind of behavior can be interpreted as in the following paragraph:

A reasonable flow of water that produces a uniform artificial rain, leads to the ejection of a few numbers of suspended water drops at each cycle of vibration. As far as the flow of water and consequently the intensity of precipitation of rain increase, the volume of water drop, before ejection, increases too. On the other hand, drops with larger radius will be created. This augmentation continues until the balance of forces applied to a drop causes to the drop ejection. This result is in agreement with the experimental results of Farzaneh

M., which are highlighted in Chapter 3 [Farzaneh M. 1986]. In this figure the amplitude of vibration (induced by corona) versus the precipitation of rain is illustrated in this chapter and it is shown that, for a precipitation of rain less than 25 mm/h, the amplitude of vibration is linearly increasing and then it keeps a constant value.

For the alternative voltage, the variation of volume of water drop before ejection is more complex than continuous voltage. Regarding Figure 4-13, the volume of drop on the AC curve has an approximate linear increment up to 20mm/h intensity of rain. Then it saturates at about 25 mm/h but some decrements are observed at intensity of 35mm/h.
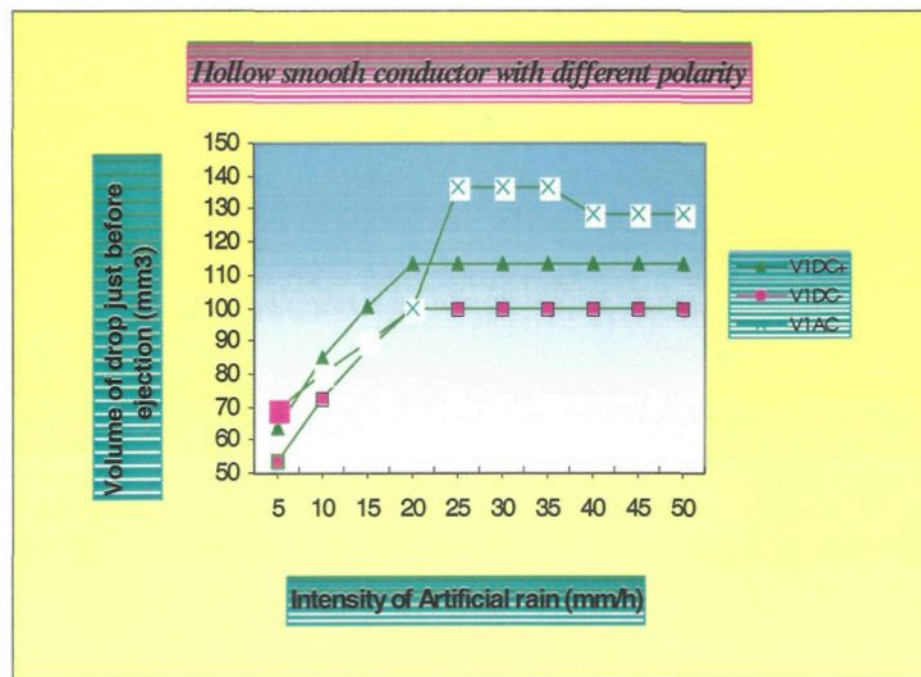
Figure 4-13: *Volume of drop just before ejection*

The alternative curve can be interpreted analogously with the DC curves except for the higher intensities. It is obvious that too much intensity of rain brings disturbances out

59

and leads to an overlap of cycles. This high intensity causes a premature ejection of the drop, before the complete evolution has taken place. This event occurs for an AC voltage because the alternating of the voltage helps to have more disturbances than DC voltage and can affect the results.

Figure 4-14, shows that the residual volume of water after ejection is constant for all the polarities and variation on the intensity of precipitation of rain. It seems that the balance of forces always keeps a fixed value for the residual volume of water drop after ejection.
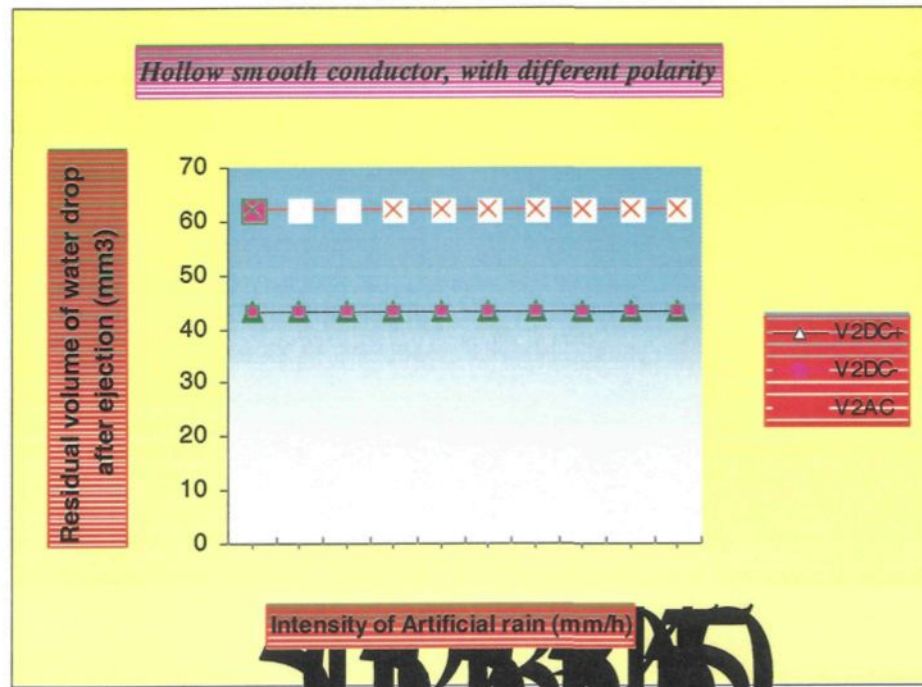
Figure 4-14: *Residual volume of water after ejection*

The Parameter K is the ratio of drop volume before and after ejection. This ratio is used for the numerical simulation presented in Chapter 5. For a specific electrical field and precipitation of rain, the K ratio and maximum volume of water drop just before ejection are entered to the numerical model as inputs. Based on this data, the program calculates the

residual volume of water after ejection and uses that result for the calculation of the applied

force to a suspended water drop under a high voltage conductor.
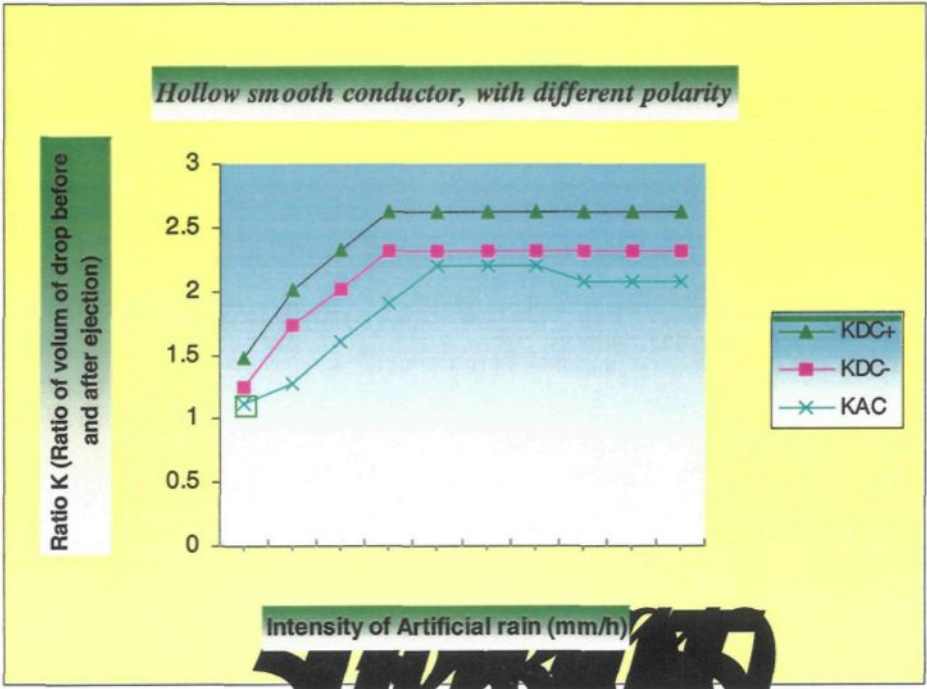
Figure 4-15: *Ratio K for hollow smooth conductor*

4.4.2   Volume of water drops on the ACSR Conductor

Figure 4-16 illustrates the volume of water drops just before ejection for the laboratory ACSR conductor.

The experimental results show that for all three polarities of the electrical field the variation curves of this volume versus the intensity of rain approximately follow the same behavior. The applied water has an intensity between 5~50 mm/h and the characteristic of the curves on this margin shows a primary increment of the drop volume versus intensity of the artificial rain and then curves reaches to the saturation point. The saturation point of the curves is actually the stop point of volume variations. For different polarities, the required saturation point is different. The AC curve has the earliest saturation, DC+ has the latest one and DC- curve stops volume variations at the highest level.

As it is mentioned for the hollow smooth conductor, a reasonable flow of water that produces a uniform artificial rain, leads to the ejection of a few numbers of suspended water drops at each cycle of vibration. As much as the flow of water and consequently the intensity of precipitation of rain increase, the volume of water drops increases. On the other hand, the drops with larger radius will be created. This augmentation continues until the balance of forces applied to a drop depresses more increments of volume. This result is in agreement with the experimental results of Farzaneh M., which are highlighted in Chapter 3 [Farzaneh M. 1986]. In this Figure, the amplitude of vibration versus the intensity of rain is

illustrated and it is shown that, for a precipitation of rain less than 25 mm/h, the amplitude of vibration is linearly increasing and then it keeps a constant value.

Figure 4-17 shows that residual volume of water after ejection is constant for all the polarities and for most variations on the intensity of precipitation of rain. It seems that the balance of forces always keeps a fixed value for the residual volume of water drop after ejection.

Figure 4-17: Residual volume of water drop after ejection
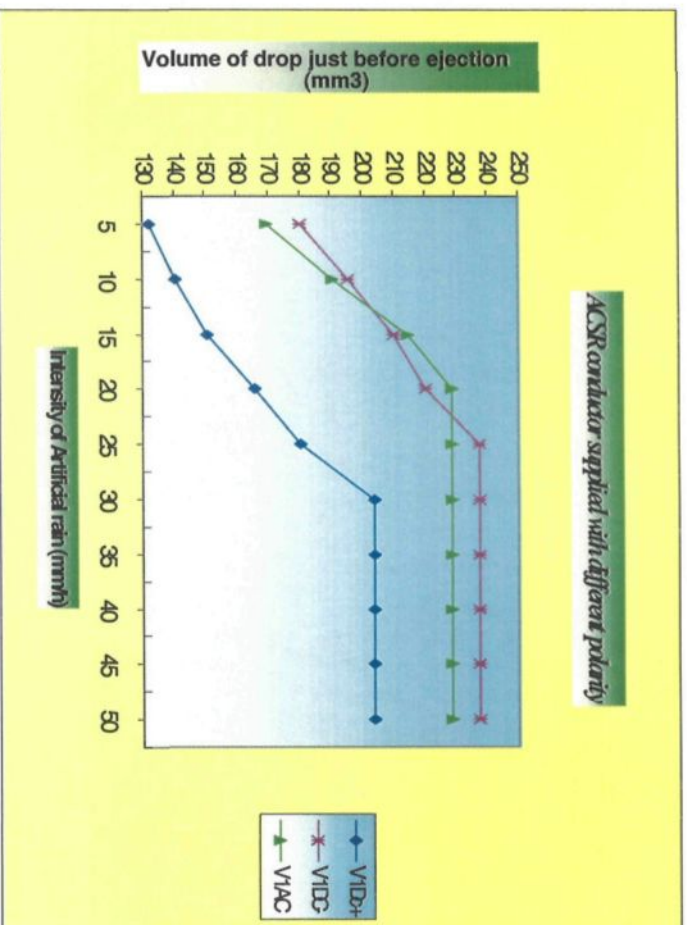
Figure 4-16: Volume of drop just before ejection

Parameter K is the ratio of drop volume before and after ejection. For numerical simulation in Chapter 5, this ratio is used. For a specific electrical field and precipitation of rain, the K ratio and the maximum volume of water drop just before ejection are entered to the numerical model as inputs. Based on this data, the program calculates the residual volume of water after ejection and uses that result for the calculation of the applied force to a suspended water drop under a high voltage conductor.
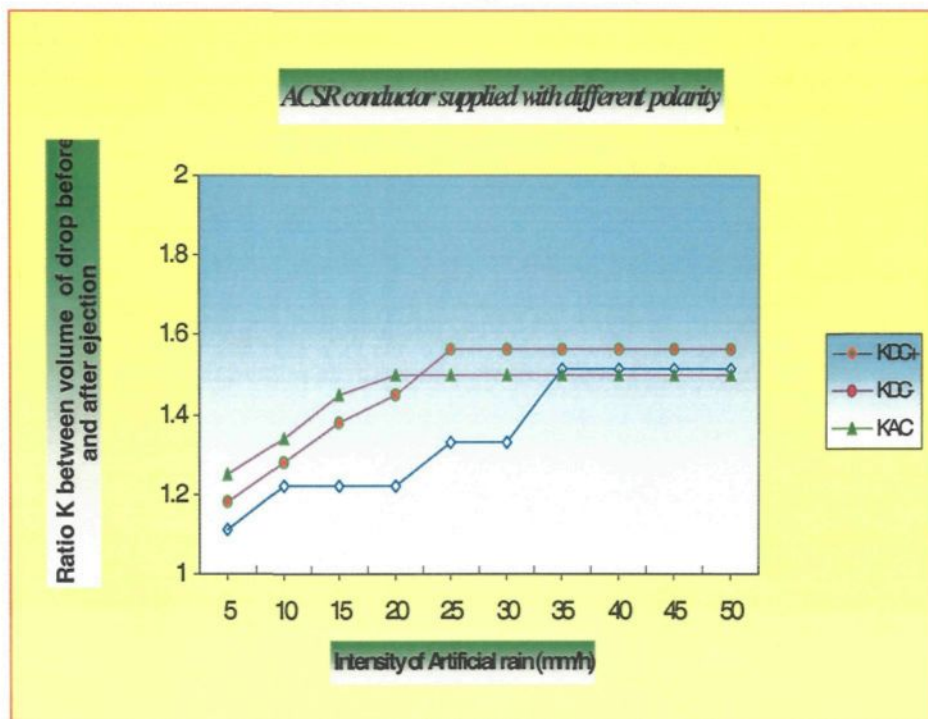

Figure 4-18: Parameter K for the ACSR conductor

The experimental results presented in this chapter provide the essential inputs (parameter K, radius of drop, volume of drop before and after ejection) for the numerical simulation.

CHAPTER 5

NUMERICAL SIMULATION

5.1. INTRODUCTION

Today, numerical modeling and simulation are powerful tools for solving complex problems. To perform a numerical simulation, input data should be applied to the numerical model. Preparing accurate data for the simulation is sometimes a milestone and due to this fact researchers find an indirect approach to require necessary information. Since, gathering necessary information on corona-induced vibration of high voltage transmission lines under precipitation of rain is arduous, different methods are adopted by researchers. A review of technical literature shows that the following approaches are more often undertaken. One approach benefits from the statistical methods that represent the inputs of a mathematical model by different distribution functions. Shah & Morgan [1976] use this technique for their research work. With the other approach, an experimental model is employed to gather some essential data for developing numerical models. Even the researchers who benefit from their experimental models use the statistical approaches for some parameters. Demers' research work could be a good example of this approach [Demers P., 1994]. However, the results show that the more inputs are defined statistically, the less precise responses are acquired.

To represent a realistic numerical model for the vibration (induced by corona) of high voltage conductors in the presence of rain, and to require the minimum inputs and acceptable outputs, the finite element method has been chosen.

The finite element method is a numerical analysis technique for obtaining approximate solutions to a wide variety of engineering problems. Although originally developed to study the stresses in complex airframe structures, it has since been extended and applied to the broad field of continuum mechanics. Because of its diversity and flexibility as an analysis tool, it is receiving much attention in engineering schools and in industry.

5.2. Theory of Finite Element

In a continuum problem of any dimension, the field variable (whether it is pressure, temperature, displacement, stress, or some other quantity) can take infinitely many values because it is a function of each generic point in the body or solution region. Consequently, the problem is one with an infinite number of unknowns. The finite element discretization procedures reduce the problem to one of a finite number of unknowns by dividing the solution region into elements and by expressing the unknown field variable in terms of assumed approximating functions within each element. The approximating functions (sometimes called interpolation functions) are defined in terms of the values of the field variables at specified points called nodes or nodal points. Nodes usually lie on the element boundaries where adjacent elements are considered to be connected. In addition to boundary nodes, an element may also have a few interior nodes. The nodal values of the field variables and the interpolation functions for the elements completely define the behavior of the field variables within the elements. For the finite element representation of

a problem, the nodal values of the field variable become the new unknowns. Once these unknowns are found, the interpolation functions define the field variable throughout the assemblage of elements.

Clearly, the nature of the solution and the degree of approximation depend not only on the size and number of the elements used, but also on the interpolation functions selected. Often functions are chosen so that the field variable or its derivatives are continuous across adjoining element boundaries.

An important feature of the finite element method that sets it apart from other approximate numerical methods is its ability to formulate solutions for individual elements before putting them together to represent the entire problem. This means, for example, that if we are treating a problem in stress analysis, we can find the force-displacement relationship or the stiffness characteristics of each individual element and then assemble the elements to find the stiffness of the whole structure. In essence, a complex problem reduces to considering a series of greatly simplified problems.

Another advantage of the finite element method is the variety of the ways in which one can formulate the properties of individual elements. There are basically four different approaches:

1. Direct approach, its origin can be traced back to the direct stiffness method of structural analysis.

2. Variational approach relies on the calculus of variations and involves extremizing a functional.

3. Weighted residuals approach, begins with the governing equations of the problem and proceeds without relying on existence of a functional or a variational statement. This approach is advantageous because it thereby becomes possible to extend the finite element method to problems where no functional is available.

4. Energy balance approach, like the weighted residuals approach requires no variational statement and hence broadens considerably the range of possible applications of the finite element method.

Regardless of the approach used to find the element properties, the solution of a continuum problem by the finite element method always follows an orderly step-by-step process.

5.3. Numerical Model

To model the corona-induced vibrations of transmission lines under rain, the laboratory model employed in chapter 4 is used. As it is illustrated on Figure 4-2, two types of conductor are located along the axis of the mesh cage for different set-ups. The hollow smooth conductor is used to simplify the model of transmission lines and the ACSR conductor represents the more realistic model. Application of high voltage on the conductors produces a superficial electrical field on the surface, however, there is still no sign of vibration. Artificial rain applied to these high voltage conductors causes a kind of vibration that is interpreted as a vibration induced by corona.

The drop profile in section 4-3 indicates that the ejection of droplets from the suspended water drops creates an upward force, which affects the balance of forces applied to that drop. The distribution of the suspended drops along the length of the conductor brings out a distributed force that leads to the vertical vibration of the conductor. The involved forces applied to a suspended water drop are explained in the following sections.

The displacement of the conductor is along the vertical axis and is of the order of centimeter for the hollow smooth conductor and of the order of millimeter for the ACSR conductor. Therefore, small displacements are a feature of this vibration study. Note that most of the explanation of this chapter is applicable for both kinds of conductors, smooth and ACSR, except for the sections that are explicitly devoted to only one of them.

With a good approximation, both the hollow and the ACSR conductors could be modeled as a linear model. The uniform composite material for the hollow smooth conductor and the non-elastic feature of the ACSR conductor combined with the small displacements for both of them are the reasons for this assumption.

The model is a dynamic model due to the fact that the position of conductor changes with time. The matrix equation of motion for a linear dynamic system is:

$$[M]\{\ddot{U}\}+[C]\{\dot{U}\}+[K]\{U\}=\{f(t)\} \qquad \text{(Eq. 5-1)}$$

Where

$[M]$ Mass matrix

$[C]$ Damping matrix

$[K]$ Stiffness matrix

$\{f(t)\}$ Time varying load vector

$\{U\}$ Displacement vector

$\{\dot{U}\}$ Velocity vector

$\{\ddot{U}\}$ Acceleration vector

5.3.1   Mode Superposition

To present a reasonable model of vibration, the first five harmonics of motion are important to be considered. These few modes of vibration are able to accurately describe the time history of the response. Because the number of modes of vibration is few (five modes) and the system is linear, Modal Superposition should be a good choice and there will be no need to use a direct integration. Once the eigenvalue problem is solved for the natural modes and frequencies, we can use the method of modal superposition to determine the solution of the complete set of equations.

The above system of equations (Eq. 5-1) is generally coupled, with [K] banded and [M] and [C] either banded or diagonal. They would be uncoupled if and only if all three matrices were diagonal. A system of uncoupled ordinary differential equations is considerably less expensive to integrate than a coupled system. The purpose of modal superposition is to transform (Eq. 5-1) into an uncoupled system in order to realize cost savings.

There are two approaches to uncouple the system of equations (Eq. 5-1). Both involve the calculation of the system of eigenvalues (frequencies) and eigenvectors (modes)

corresponding to this system of equations. One approach calculates the undamped modes and the other approach calculates the damped modes. The latter is an exact method with no simplification regarding the damping factor but is more expensive. The former approach must make simplifying assumptions regarding the damping, but the assumptions are appropriate for many common structural applications. Consequently, the undamped mode approach is currently the standard approach in virtually all-commercial FE structural programs and will be described below.

The undamped modes for (Eq. 5-1) are the time-harmonic (sinusoidal) solutions when there are no loads ({F}={0}) and damping is neglected ([C]=[0]); that is,

$$[M]\{\ddot{a}\} + [K]\{a\} = \{0\} \qquad \text{(Eq. 5-2)}$$

Let
$$\{a\} = \{v\}e^{i\omega t} \qquad \text{(Eq. 5-3)}$$

Substituting (Eq. 5-3) into (Eq. 5-2) yields:

$$[K]\{v\} - \omega^2 [M]\{v\} = \{0\} \qquad \text{(Eq. 5-4)}$$

Which is the generalized algebraic eigen problem where the eigenvalue λ is the square of the circular frequency, that is, $\qquad \lambda = \omega^2$

If the system has N eigen solutions:

$$\left(\omega_1^2, \{v\}_1\right), \ \left(\omega_2^2, \{v\}_2\right), \ ..., \ \left(\omega_N^2, \{v\}_N\right)$$

where
$$0 < \omega_1^2 \le \omega_2^2 \le ... \le \omega_N^2$$

, and the eigenvectors are orthogonal with respect to [K] and [M], and they are orthonormal with respect to [M]; that is,

$$\{v\}_i^T [K]\{v\}_j = \omega_i^2 \delta_{ij}$$

(Eq. 5-5)

$$\{v\}_i^T [M]\{v\}_j = \delta_{ij}$$

It is convenient to define an N-by-N square matrix [V] that contains the N eigenvectors as

columns:
$$[V] = [\{v\}_1, \{v\}_2, ..., \{v\}_N]$$

and an N-by-N diagonal matrix $[\Omega^2]$ that contains the N eigenvalues on the diagonal.

With this notation, we may compactly write all N solutions to (Eq. 5-4) as follows:

$$[K][V] = [M][V][\Omega^2]$$

And the orthogonality relations (Eq. 5-5) may be written

$$[V]^T [K][V] = [\Omega^2]$$

(Eq. 5-6)

$$[V]^T [M][V] = [I]$$

where [I] is the identity matrix. This system of N modes can now be used to transform the

following non-homogeneous system of equations:

$$[M]\{\ddot{a}\} + [C]\{\dot{a}\} + [K]\{a\} = \{F\} \qquad \text{(Eq. 5-7)}$$

The general solution to (Eq. 5-7) may be written as a linear superposition of the N modes,

each multiplied by a general time varying amplitude:

$$\{a(t)\} = \sum_{j=1}^{N} A_j(t)\{v\}_j \qquad \text{(Eq. 5-8)}$$

$$= [V]\{A(t)\}$$

Substituting (Eq. 5-8) into (Eq. 5-7), pre-multiplying the latter by $[V]^T$, and using (Eq. 5-6)

yields:

$$\{\ddot{A}\} + [V]^T [C][V]\{\dot{A}\} + [\Omega^2]\{A\} = [V]^T \{F\} \qquad \text{(Eq. 5-9)}$$

The initial conditions $\{a\}_0$ and $\{\dot{a}\}_0$ are transferred to $\{A\}$ by pre-multiplying (Eq. 5-8) by $[V]^T[M]$; that is,

$$\{A\}_0 = [V]^T[M]\{a\}_0$$

$$\{\dot{A}\}_0 = [V]^T[M]\{\dot{a}\}_0$$

Equations (Eq. 5-9) are the transformed system equations. The DOF are now the amplitudes of each mode. The stiffness and mass terms have been uncoupled, but the damping term remains coupled for arbitrary $[C]$. When damping cannot be neglected, it is a good assumption that $[V]^T[C][V]$ is diagonal and equals to:

$$[V]^T[C][V] = [C_D] \qquad \text{(Eq. 5-10)}$$

where $2\omega_i\xi_i$ are at the diagonal of this matrix. ξ_i are the modal damping ratios, which are the percent of critical damping in each mode. Substituting (Eq. 5-10) into (Eq. 5-9) uncouples the latter, enabling them to be written as N separate equations:

$$\ddot{A}_i(t) + 2\omega_i\xi_i\,\dot{A}_i(t) + \omega^2 A_i(t) = f_i(t) \qquad i=1,2,..,N \qquad \text{(Eq. 5-11)}$$

System equations of (Eq. 5-11) can be numerically solved using one of the time-stepping methods, and then each $A_i(t)$ summed according to (Eq. 5-8) to produce $\{a(t)\}$.

5.3.2   Time Stepping Methods

We seek a recurrence relation that relates the unknown values at t_n to the known values at one or more previous times like t_{n-1} and t_{n-2}. Four of the most popular recurrence relations currently used in commercial FE programs are as follows:

- Central Difference Method

- Houbolt Method

- Wilson Method

- Newmark Method

The Newmark method is an implicit time integration method that is unconditionally stable. For this reason this method has been used to solve the system of equations (Eq. 5-11). The Newmark method assumes that the average acceleration over an integration time step is constant which is a reasonable assumption for our situation. Then, using the initial conditions at the beginning of the time step, the displacement and velocity at the end of the time step are predicted using constant-acceleration formulas.

This is a one step method in which $\{A(t)\}$ is approximated by a cubic polynomial:

$$\{A(t)\} = \{c_0\} + \{c_1\}t + \{c_2\}t^2 + \{c_3\}t^3 \qquad \text{(Eq. 5-12)}$$

Which is defined only over the current time step. The coefficients $\{c_0\}$ and $\{c_1\}$ are determined by interpolating $\{A(t)\}$ and $\{\dot{A}(t)\}$ at time step t_{n-1}. The Newmark method is a two-parameter (γ and β) family of algorithms. $\gamma = \dfrac{1}{2}$ and $\beta = \dfrac{1}{4}$ are the parameters used on this model which gives the following results:

$$\{A(t)\} = \{A\}_{n-1} + \{\dot{A}\}_{n-1}(t - t_{n-1}) + \frac{1}{2}\left(\frac{\{\ddot{A}\}_{n-1} + \{\ddot{A}\}_n}{2}\right)(t - t_{n-1})^2$$

$$\{\dot{A}(t)\} = \{\dot{A}\}_{n-1} + \left(\frac{\{\ddot{A}\}_{n-1} + \{\ddot{A}\}_n}{2}\right)(t - t_{n-1})$$

$$\{\ddot{A}(t)\} = \frac{\{\ddot{A}\}_{n-1} + \{\ddot{A}\}_n}{2}$$

5.3.3 Force Calculation

As mentioned in section 4-3, suspended water drops on the high voltage conductor are under different forces. While the forces are in equilibrium, the drop sticks to the conductor, however, the elongation of the drop compensates the downward forces, which are getting stronger due to the increasing volume of the drop. This situation continues until the resultant of the downward forces become larger than the upward forces. At this moment, the ejection of the droplet occurs. A portion of the drop that is ejected is called droplet. Due to the ejection of the droplet an upward reaction force acts on the high voltage conductor and causes a vertical displacement. At this time, the inertial force and the gravity force return the conductor back to the balance position and the conductor becomes ready to accumulate water to drops again. This process repeats itself intermittently and leads to the vibration of the high voltage conductor under rain. The frequency of vibration (induced by corona) is the same as the natural frequency of that conductor. The natural frequency depends on the boundary conditions and degrees of freedom, which are the subjects of the numerical simulation section.

The following forces are involved in the force balance of a suspended water drop on a high voltage conductor under vibration:

- ➢ Gravity force

- ➢ Inertia force

- ➢ Electrostatic force

- ➢ Tension of surface

- ➢ Induced force by Corona

- The gravity force of one drop is considered as:

$F_{Gravity}$ = Mass of Drop × Gravity Acceleration

= Density of Water × Volume of Drop × Gravity Acceleration

The density of water and the acceleration of gravity are constant, but the volume of drop is variable. The amount of drop volume at time (t) is a function of its value at time (t-1), type of conductor, polarity of electrical field, and precipitation of rain. The characteristics of these changes were described in chapter four.

- The inertia force produces a resistance to any change in the motion of a body. Because of the vibrating motion, this kind of force exists and is related to the acceleration of motion and the volume of the drop at each moment.

$F_{inertia}$ = Mass of Drop × Motion Acceleration

= Density of Water × Volume of Drop × Motion Acceleration

The density of water is constant and the volume of the drop is as explained above. Motion acceleration is calculated by the second derivative of displacement while displacement is the result of (Eq. 5-8) and is already explained.

• The electrostatic force on a suspended drop under a high voltage conductor is due to the ionization of water molecules. Depending on the polarity of the applied voltage, the type of accumulated electrical charges on the outer surface of the drop changes. It is obvious that this force is a function of the electrical field and the volume of drop [Maaroufi, 1989, p68-69]:

$$F_{Electro} = \frac{9\pi\varepsilon_0}{4}r^2 E_0^2$$

where r is the **average radius** of the suspended water drop with a value very smaller than radius of conductor, E_0 is the value of the electrical field on the surface of conductor, and ε_0 is equal to:

$$\varepsilon_0 = \frac{1}{36\pi}\times10^{-9} \qquad F/m$$

which it comes to:

$$F_{Electro} = 6.25\times10^{-11}E^2 r^2 \quad N/m$$

This force plus the gravity force lead to the elongation of the drop. For this reason as the electrical field increases, the drops will be elongated faster and it leads to an earlier ejection.

- The surface tension is related to the adhesive force between the water drop and the surface of the conductor, which resist against the separation of the water droplet from the water drop.

$$F_{Tension} = 2\pi\, r\, \gamma$$

where $\gamma = 7.28e - 02$ N/m at 20 degree centigrade.

- The force induced by Corona is due to the charge carriers moving from a high voltage conductor under rain to ground. These carriers consist of molecular ions produced by the corona discharge and the water drops, which eject from the conductor or are charged on their way to ground.

The corona phenomenon and its effect on the transmission lines under rain are explained in detail in chapter 2.

Farzaneh has measured the value of this force at the ejection time for each drop [Farzaneh M. 1986] and he reported this value as:

$$F_{Corona} = 5 \times 10^{-4} N/drop \ (\text{or } 10^{-3}\ N/two\ drops)$$

When the sum of the force induced by the corona and the adhesive force becomes larger than the sum of the three other forces (Inertia, gravity, and Electrostatic), the ejection of the water drop occurs.

5.4. Numerical Simulation

To simulate the numerical model selected in the previous section (5-3), the COSMOS/M package is used. Cosmos is a complete, modular, self-contained finite element

system developed by Structural Research and Analysis Corporation (SRAC) for personal computer and workstations (for more information on this commercial FE software refer to Cosmos User Manuals).

5.4.1 Geometry

The geometry of the model is designed based on the laboratory conductors described in chapter four. For the smooth conductor with 4.0 m length, 3.2 cm diameter, and 0.2 cm thickness, a line equal to 4.0 m is considered. For the ACSR conductor with 4.11 m length and 3.05 cm diameter, a straight line equal to 4.11 meters is considered. However, to make the model more similar for both the smooth and the ACSR conductors, the number of nodes to mesh the conductors is the same.

The middle part of these conductors, which is surrounded by a cage, is meshed with a larger number of elements to obtain more information on the dynamic motion (54 elements for middle section and 26 elements for each side). There are two nodes per element therefore, the sum of nodes for the length of the conductors, after merging the nodes, comes up to 110 nodes.

5.4.2   Element type and Natural Frequencies

Investigation on the types of existing elements in Cosmos shows that the beam element is the closest type of element for the smooth conductor and Truss2D is an adequate type for the ACSR conductor.

5.4.2.1. Beam Element

A three dimensional beam element with an aluminum alloy material type, for the actual length of the laboratory hollow smooth conductor has been selected. Also the following assumption is considered: small displacement, thin beam with circular section. The direction of force and displacement vectors to the right and upward are positive at each end of the element. Moment and rotation in the counter clockwise direction are positive at each end.

Each node can have six degrees of freedom. The first three degrees are related to the translation in directions X, Y, and Z and the three others are related with the rotation about these axes.

Compared with the geometric dimensions of the laboratory model, the smooth conductor is constrained on the nodes 62 and 103 close to the ends. Translation of the conductor in the laboratory is fixed at one side (node 62) while it can rotate about the Z-axis. At the other side (node 103), there is free displacement, dof (degree of freedom), in the X direction while the node is able to rotate about the X-axis.

The moment of inertia is calculated in each direction for the circular cross section conductor. Regarding the 0.2 cm thickness of the hollow conductor and the length of 4.0 m, the mass of the smooth conductor is 2.036 kg for 108 nodes. Then the moment inertia of each node comes to:

$$I = mr^2 = (2.036 / 108) \times (0.014)^2 = 3.72e\text{-}6 \ \text{kg.m}^2$$

The stiffness matrix is built according to these situations where:

$$U_y = \frac{f_y L^3}{3EI}$$

L is the beam length, E is Young's modulus of elasticity, and I the nodal moment inertia.

The mass matrix is calculated for the beam elements while the mass of each element is located at the center of that element.

The natural frequencies of the smooth conductors are calculated by Cosmos software according to the specified characteristic and they are as follows for the first five modes:

$F_1 = 7.91392$ Hz

$F_2 = 11.5014$ Hz

$F_3 = 25.564$ Hz

$F_4 = 31.704$ Hz

$F_5 = 53.0417$ Hz

The frequency of vibration (induced by corona) measured by oscilloscope is about 7.9 Hz that is the first natural frequency of the smooth conductor.

5.4.2.2. Truss Element

A 2-node uniaxial Truss element with aluminum alloy material type, for the actual length of the laboratory ACSR conductor has been selected. Also the following assumption is considered: small displacement with linear elastic material type. All the elements are defined in the X-Y plane with only two translational degrees of freedom per node.

Moment of inertia per each node is calculated as follows:

$$V = \pi r^2 L = \pi (3.05/2)^2 \times 411 = 0.003 \ m^3$$

$$M = \rho \ V = 2700 \times 0.003 = 8.1 \ kg$$

$$I = m \ r^2 = (8.1 / 108) \times (0.015)^2 = 1.69e\text{-}5 \ \ kg.m^2$$

By performing the frequency analysis, the following natural frequencies have been obtained for the ACSR conductor:

$F_1 = 5.80228$ Hz

$F_2 = 13.3999$ Hz

$F_3 = 21.8452$ Hz

$F_4 = 36.9367$ Hz

$F_5 = 42.8728$ Hz

The frequency of vibration (induced by corona) measured by oscilloscope is about 5.9 Hz that is the first natural frequency of the ACSR conductor

5.4.3 Static Analysis

Static analysis deals with the computation of displacement strains and stresses due to the static loading. The term static load refers to the loading that does not cause inertial or damping effects to be significant for consideration in the analysis. Static analysis is linear if non-linearities can be either linearized or completely ignored. The stress-strain relationship for linear analysis is linear, and so is the relation between the load and deflection. Therefore, doubling the load vector for a problem will result in doubling all the results associated with it.

In this numerical simulation, static analysis is applied only to prepare initial values for the start up of dynamic analysis. Due to the inertia force explained in section 5.3.3, this force has a non-zero value if the displacement vector has an initial value. Then all the applied forces to a suspended water drop are available and dynamic analysis can start with a real status of vibration.

Applied forces to the static analysis are distributed along the length of conductor with a distance of about nine drops. According to the report of Farzaneh, for every cycle of vibration, for each meter of the conductor there is a possibility of 27 drops which 9 of them are elongated [Farzaneh M. 1986]. While a drop is suspended and elongated, the corona force around that drop has its maximum value. With regards to this information, 7 vertical forces equal to the force-induced by corona applied to the conductor and the result of static analysis came up with a good initial condition to start up the inertia force.

5.4.4 Dynamic Analysis

Dynamic problems are characterized by governing differential equations that contain a second-order time derivative, $\dfrac{\partial^2 U}{\partial t^2}$. This term is due to inertial forces, which are the essential feature of a dynamics problem and is explained in section 5-3-3.

The advanced dynamic analysis of Cosmos program is based on the normal modes method. Therefore, the frequencies and mode shapes calculations are done prior to the application of this dynamic module.

To start a dynamic simulation, a desire precipitation of rain and of electrical field on the surface of conductor is chosen. At each time step (0.02 sec), one node from the middle section of the conductor, which is surrounded by the cage and is under precipitation of artificial rain, is randomly selected. Depending on the rain precipitation, a specific amount of water is added to the previous volume of the selected drop. Then the applied forces to each node of the middle part of the conductor (55 nodes) are calculated. By this method the curve defining the time variation pattern of the load is defined.

For a dynamic analysis by Cosmos, the change of load versus time should be pre-defined at the beginning. But, according to the forces applied to the suspended water drops, values of these forces at time t are functions of the drop volume and of the displacement of the conductor at time step (t-1). Therefore, the program should execute somehow to generate the forces at each time step. This job became possible by generating an initial value from static analysis. The results of the static analysis are applied to the internal loop,

which is developed to calculate the involved forces for each node, and the value of forces

for the time step (t + 1) has been calculated.

When the forces on each drop are calculated, the balance of them is considered as a

result. If this balance is larger than zero it means that the drop is ejected. Due to the

complex procedure of forces involved in this phenomenon, instead of applying the resultant

force continuously, a force equivalent to an impulse force will be applied. Demers

formulated the impulse force versus the sinusoidal force [Demers P. 1994 , page 35].

According to that formula and by substituting the existing values for this model, the

coefficient transferring a continuous force into an equivalent impulsive force is equal to

33.55. Therefore at the moment of ejection of each drop, this equivalent force will be

applied to that node. By this method, dynamic analysis is performed for each node and at

each time step.

5.4.5   Post-processing results

Post-processing of the system response for the different dynamic conditions can be

performed with Cosmos software. Graphical depiction or numerical listing of the time or

frequency dependent responses can readily be obtained for any part of the structure or for

any time or frequency step.

Regarding the numerical models for the smooth and ACSR conductors, two series

of numerical simulations have been performed and consequently two sets of post

processing results have been obtained. To have a brief summary of these results, some

figures are drawn for both the smooth and the ACSR conductors. *Note that the figures shown in this section are drawn just for one period of time and they will be repeated by increasing the time margin. Also the damping factor is applied for all the results (refer to 5.4.6).*

As a post processing result, the nodal displacements of six scattered nodes along the smooth conductor is shown in Figure 5.1. In this Figure, the foregoing vertical vibration from one side of the conductor to the middle and then to the other side of the conductor is illustrated for a period of 1.2 seconds. This nodal displacement is taken for an AC electrical field of 14 kV/cm.
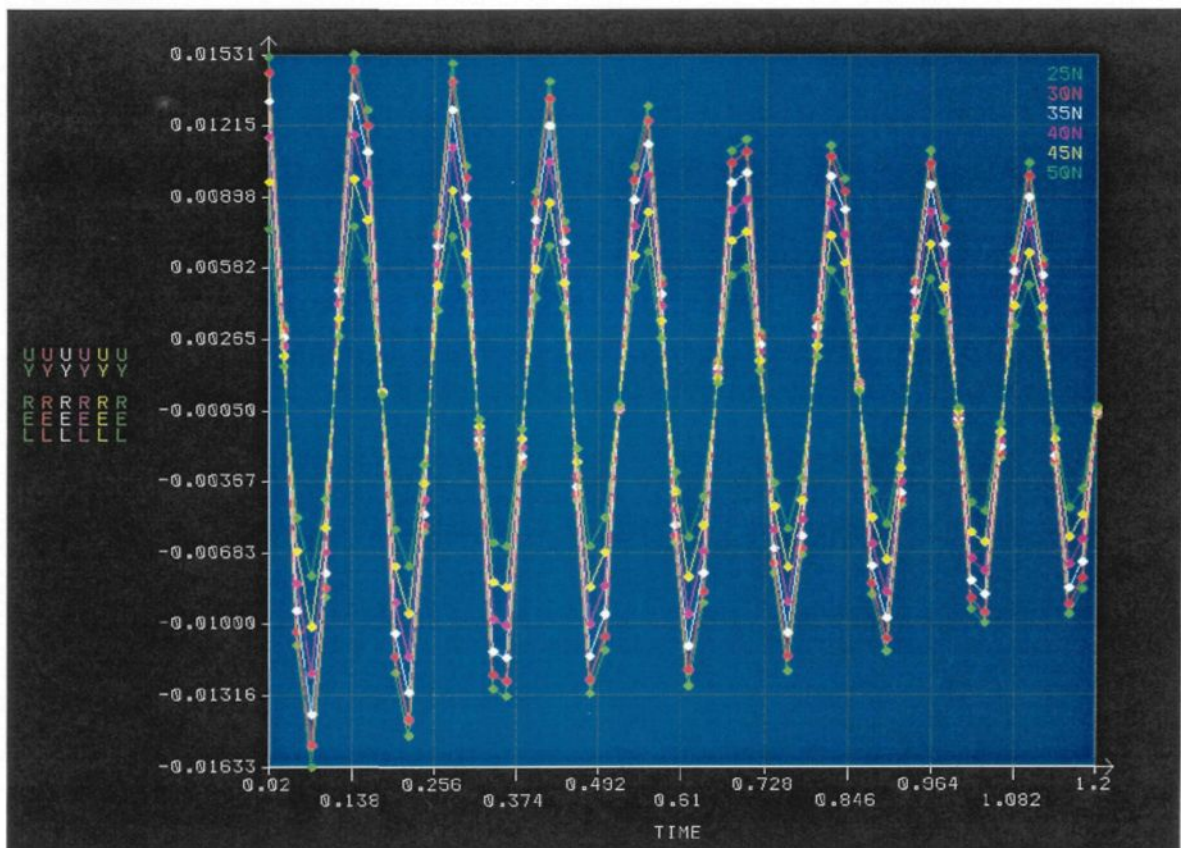

Figure 5-1: Nodal displacements of the smooth conductor (AC, 14 kV/cm)

Figures 5-2 and 5-3 show the acceleration and the displacement of the vibration of the smooth conductor under negative DC voltage with a superficial electrical field of 16 kV/cm. On these figures, the horizontal axes are time (Second) and the vertical axes are amplitude of acceleration and displacement (Meter). These curves are the results of executing the numerical simulation for a period of 1.2 second. A damping factor related to the real condition is applied to the simulation, which has a damping effect on the curves.

By comparing these two curves at the same time steps, it concludes: when the high voltage conductor under the rain is at the highest position, its acceleration is maximal. Help of our observations in the laboratory can interpret this result as follows. Due to the reactive force produced by this acceleration, the water drops become flat on the surface of the conductor (observation). Therefore, the ionization of the air is relatively weak at this position. When the conductor moves downward, the amplitude of acceleration decreases and reaches zero at the balance position which is the position of the conductor before vibrating. At this position, the acceleration's vector is upward and the water drops start to lengthen. From this point, while the conductor is going downward, the discharge current becomes more larger until the length of water drop becomes critical. This is the time for the water drop ejection and the conductor is at its lowest position. The reaction force due to the ejection of water drops sends the conductor upward and the process repeats again.

Figures 5-4 and 5-5 show the acceleration and the displacement of vibrating ACSR conductor under positive DC voltage with a superficial electrical field 15 kV/cm.

Different behaviors of the smooth conductor and the ACSR conductor are the subjects of upcoming pages.
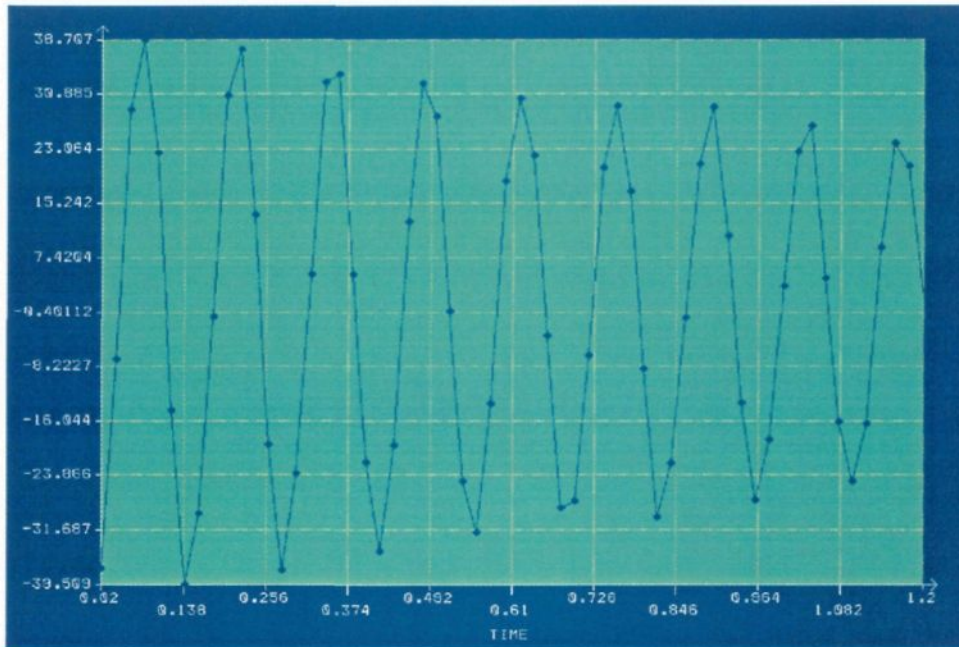
**Figure 5-2:** *Acceleration of the smooth conductor,(DC-, 16 kV/cm)*
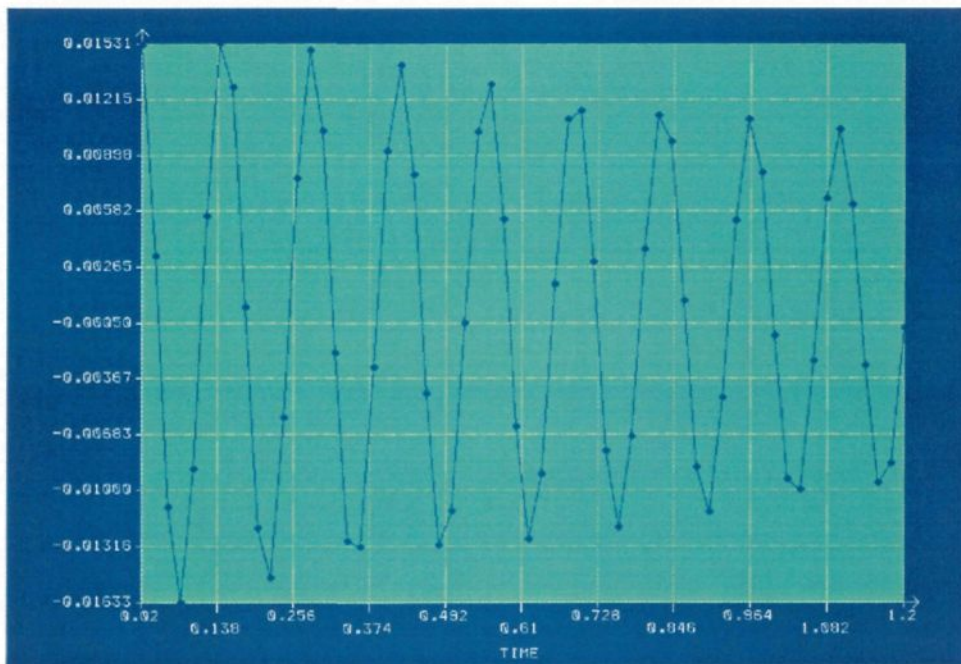
Figure 5-3: *Displacement of the smooth conductor, (DC-, 16 kV/cm)*
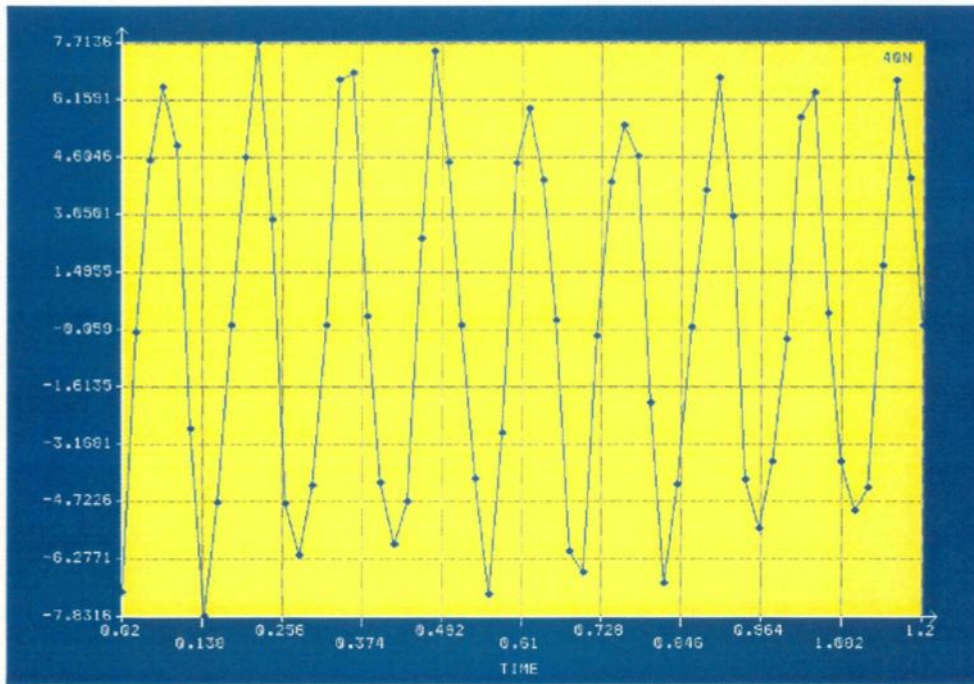
Figure 5-4: *Acceleration of the ACSR conductor (DC+ 15 kV/cm)*
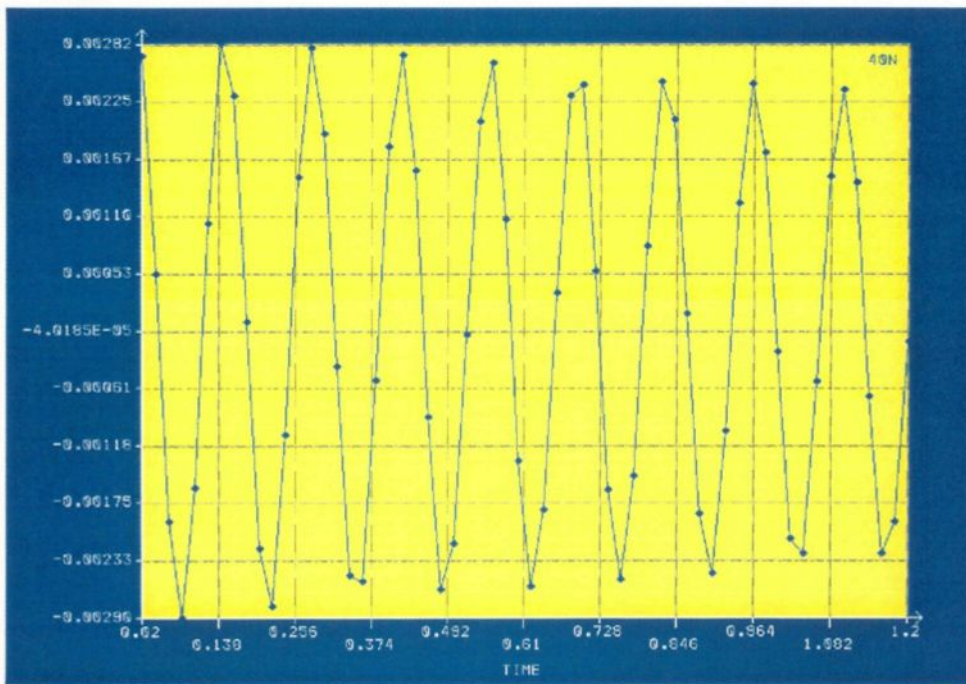
Figure 5-5: *Displacement of the ACSR conductor (DC+ 15 kV/cm)*

### 5.4.6 Damping Factor

Damping is generally present in all oscillatory systems. Its effect is to remove energy from the system. Energy in a vibrating system is either dissipated into heat or radiated away. In vibration analysis, we are generally concerned with damping in terms of system response. The loss of energy from the oscillatory system results in the decay of the amplitude of free vibration. In steady-state forced vibration, the loss of energy is balanced by the energy supplied by the excitation source. A vibrating system may be subjected to several types of damping forces, ranging from internal molecular friction to air friction. Generally, their mathematical description is quite complicated and not suitable for linear vibration analysis. Therefore, simplified damping models have been developed, which in many cases have been found to be adequate in evaluating the system response.

Maaroufi has used a curve of the damping factor versus the frequency reported by C.I.G.R.E. [Maaroufi M., 1989, page 104]. This curve shows that an ACSR conductor with frequencies of vibration under 20 HZ has a critical damping factor less than 0.1% and larger than 0.04%. The damping factors used for the numerical simulation are based on this curve and the results for the smooth conductor and the ACSR conductor are shown in Figures 5-6 and 5-7.

By comparing these two Figures one can conclude that the damping effect on a smooth conductor is more than an ACSR conductor. It means the damping of the amplitude

of vibration is faster on a smooth conductor which is the same as experimental results

developed by Farzaneh [Farzaneh M., 1986, page 113].
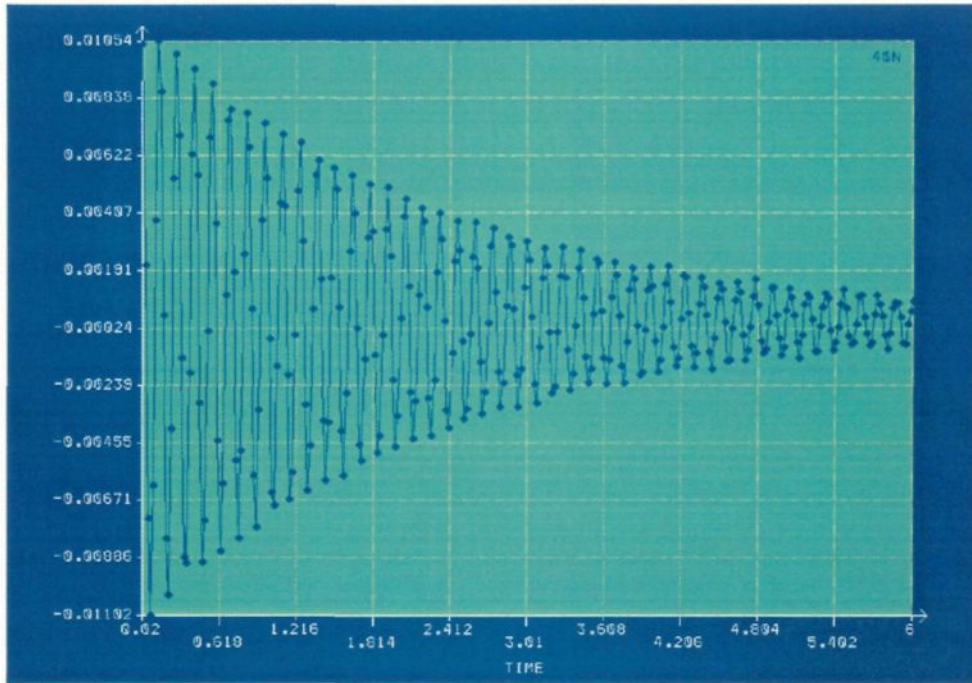
Figure 5-6: *Applied damping factor on the smooth conductor*
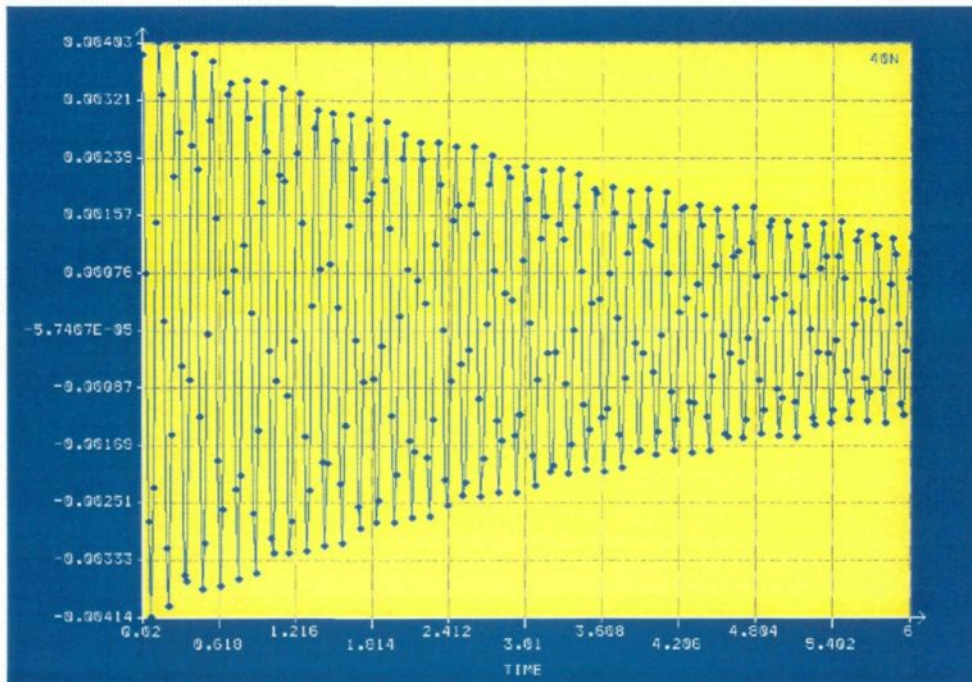
**Figure 5-7:** *Applied damping factor on the ACSR conductor*

The following figures (5-8 to 5-9) illustrate the amplitude of vibration of the smooth and the ACSR conductors supplied by different polarities of the electrical field under a rain precipitation of 25 mm/h. These amplitudes for the smooth conductor are expressed per Centimeter and for the ACSR conductor is per Millimeter. The curves show the behavior of these two types of conductors under voltage of alternative, positive, and negative supply. The numerical simulations are performed for a superficial electrical field ranging from 13 to18 kV/cm. This range of the superficial electrical field is the most likely one on the conductors of real transmission lines. A precipitation of 25 mm/h is considered to eliminate the variation of amplitude due to precipitation of rain [Farzaneh M., 1986, page 50].

Based on the results illustrated in Figure 5-8, the amplitude of vibration of the hollow smooth conductor is maximal for an alternative electrical field and is minimal for negative DC. The changes of amplitude are the same for an electrical field between 13~14 kV/cm and is close to linear for all types of polarities.

It is shown on Figure 5-9 for the same value of the electrical field supplied to the ACSR conductor, negative DC has the most amplitude of vibration and alternative has the less. These results can be explained by the fact that at the same applied voltage, corona activities in the air are usually stronger under negative fields than under positive fields because of the lower negative corona-onset voltage. The relatively low amplitude of the vibration under AC fields, compared to that under DC, may be attributed to the residual corona-space charge from the previous half cycle of each period of instantaneous voltage.

The nonlinearly on the curves of this figure refers to the different behavior of ACSR conductors in comparison to smooth conductors.
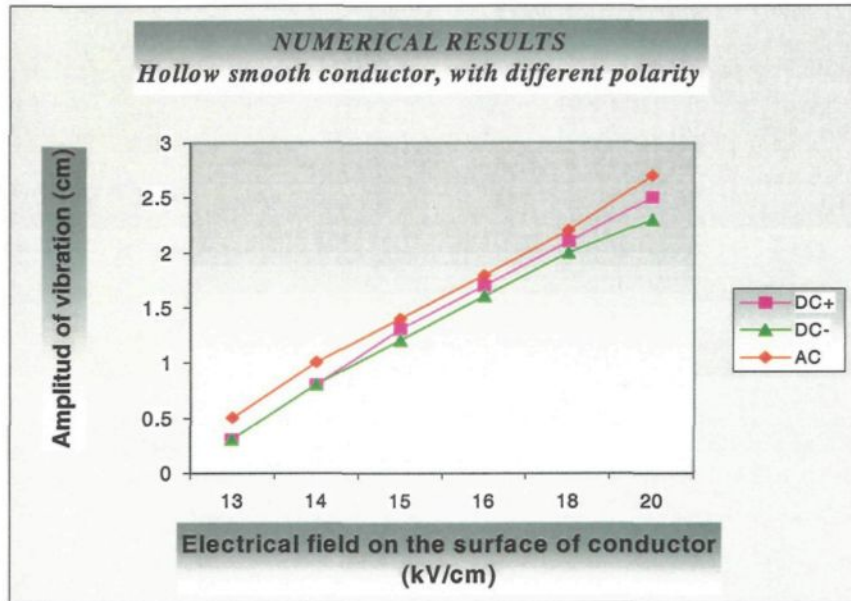
Figure 5-8: *Vibration of smooth conductor for different polarities*
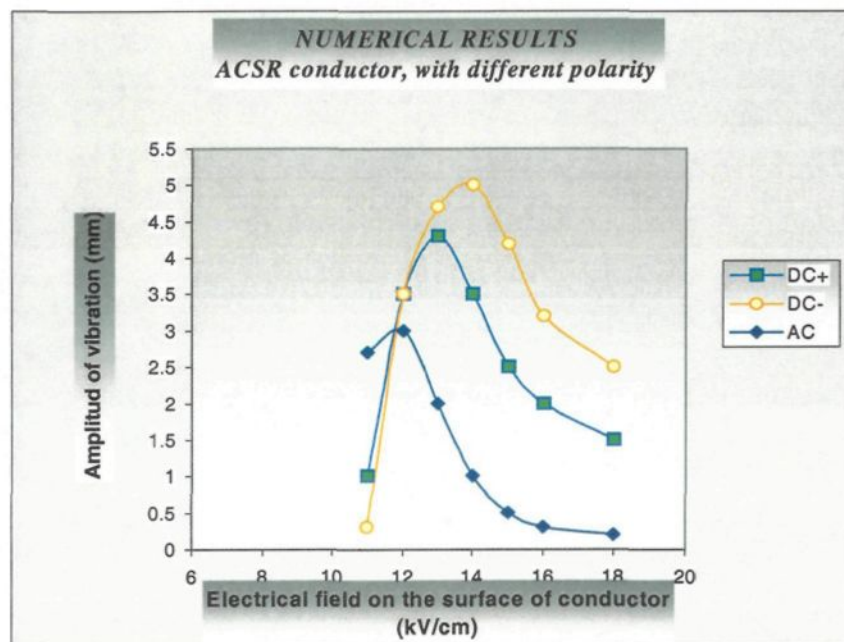
Figure 5-9: *Vibration of ACSR conductor for different polarities*

CHAPTER 6

VALIDATION

6.1. Introduction

Following the post processing of the numerical simulation and the generation of all the required results, the final step is to validate the obtained results.

To validate the numerical simulations that have been presented earlier, it is an adequate way to compare the numerical results with the experimental results obtained for the same conditions and situations. Since our numerical model is based on the physical model used by Professor Farzaneh, a comparison of the numerical results with his results would be the best choice.

The validation of the results and consequently the validation of the numerical model is performed using two different experimental set-ups. The first set-up is for the smooth conductor and the second one for the ACSR (Aluminum Conductor Steel Reinforced) conductor.

6.2. Smooth Conductor

The hollow smooth conductor described in chapter four would behave differently under tension of different electrical field polarities. Figures 6.1, 6.2, and 6.3 illustrate the variation of the amplitude of vibration induced by corona for the following polarities:

1) Alternative

Figure 6-1 shows the reactions of the smooth conductor produced by varying the AC electrical field and under a rain precipitation rate above 25mm/h. The curves are shown for both the numerical and the experimental simulation. The numerical curve is drawn in red color and the experimental in magenta. The amplitude of vibrations for both simulations are the same at 13kV/cm superficial electrical field. Then for the higher field intensity, the curves slightly separate. The highest divergence occurs at 18.5kV/cm electrical field with a difference of about 0.3cm. It should be noted that creating the exact same conditions for two successive experimental simulations is hard and the results are slightly different. For this research work we tried to compare the numerical results with the most occurred experimental results.
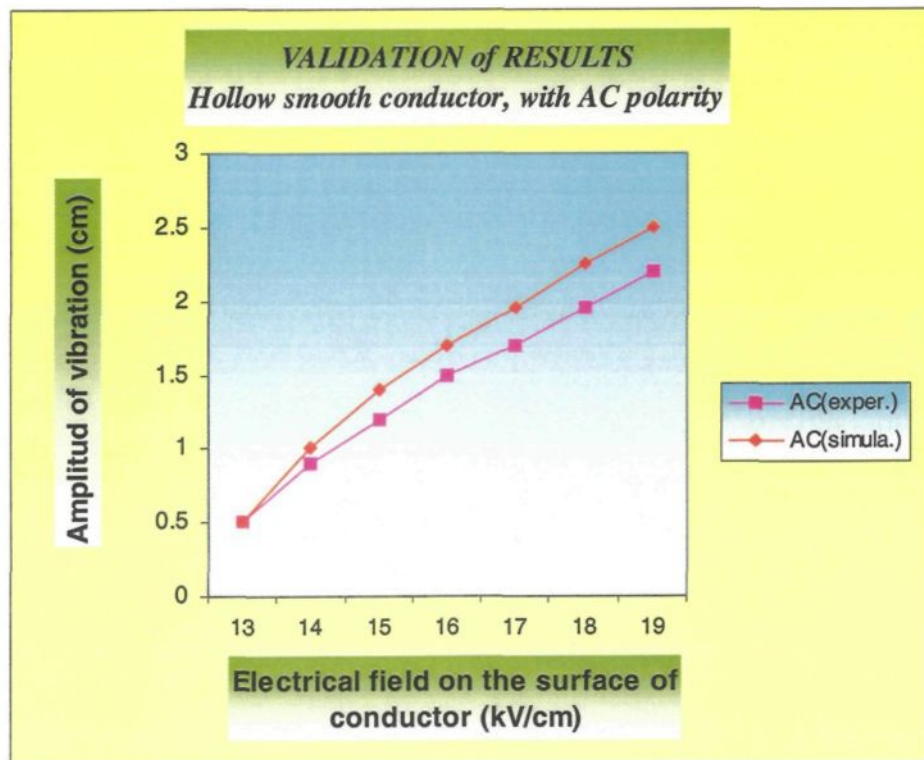
Figure 6-1: *Comparison of numerical and experimental results for the smooth conductor supplied by AC electrical field*

Figure 6-2 and Figure 6-3 show the results of simulation for the smooth conductor described in chapter four. The simulations are performed with the same conditions as in previous simulation illustrated by Figure 6-1 except for the type of polarity of charge.

2) DC positive

On Figure 6-2, which illustrates the amplitude of vibration of the smooth conductor supplied by DC+, the cyan curve shows the numerical simulation results and the yellow curve the experimental results. The numerical curve agrees with the experimental curve for a superficial electrical field between 13~14 kV/ cm. Then the two curves diverge slightly but still follow the same behavior. It seems that the numerical model has been properly designed since it matches with the experimental results. At the worst case, there is a 0.3cm divergence.

3) DC negative

Figure 6-3 shows the behavior of the smooth conductor charged by negative DC. The magenta curve shows the numerical simulation results and the green curve the experimental results. The numerical curve agrees with the experimental curve for a superficial electrical field between 13~14 kV/ cm. Then they diverge slightly but still follow the same behavior, which indicates that a good numerical model was used. At the worst case, there is a 0.3cm divergence for the amplitude of vibration.
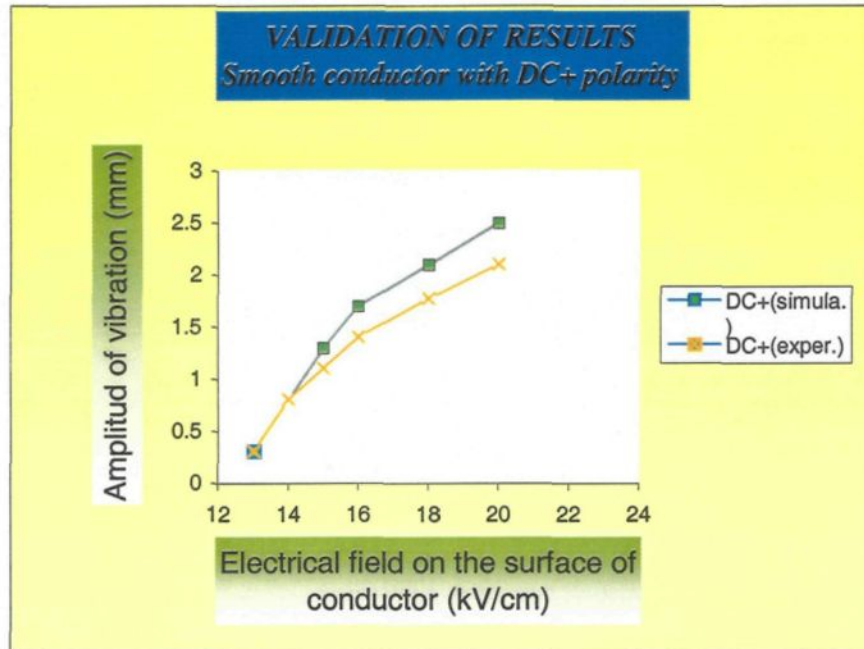
Figure 6-2: *Smooth conductor supplied by DC+*
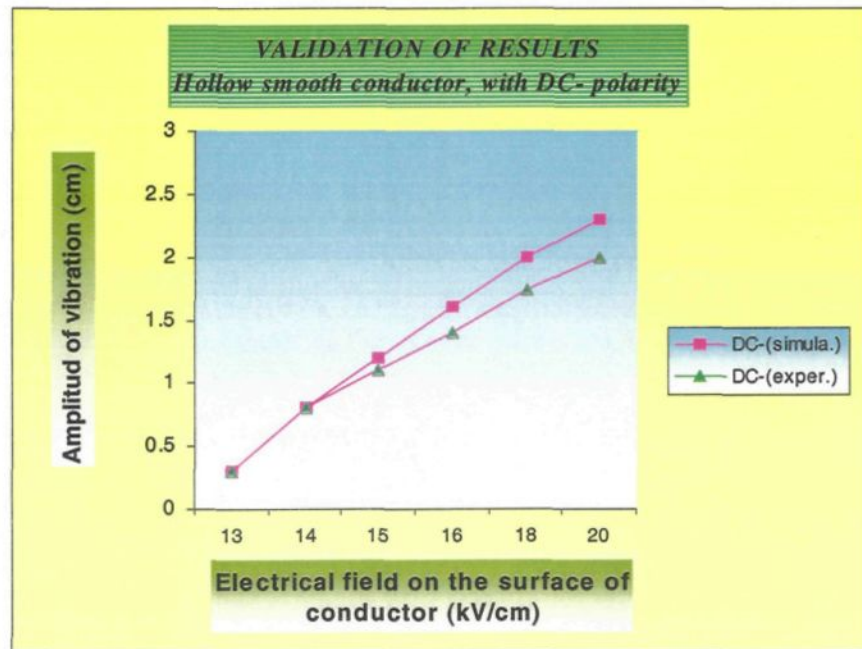

Figure 6-3: *Smooth conductor supplied by DC-*

6.3. ACSR Conductor

Now that our numerical model for the smooth conductor satisfies the desired precision, it is the time to verify the accuracy of a more complicated model for the ACSR conductor described in chapter four. As the geometry, material, and element type for this kind of conductor is different from the hollow smooth conductor, we are expecting different results but likely similar to the experimental results obtained from the similar laboratory conditions.

The following sections compare the behavior of the ACSR conductor, described in chapter four, for different simulations and under various polarities of the electrical field. Note that the amplitude of vibration is expressed in per millimeter.

1) Alternative

On Figure 6.4, the amplitude of vibration induced by corona of the ACSR conductor supplied by the AC electrical fields is shown. The conductor is considered under a rain precipitation rate above 25mm/h. The numerical curve is cyan and the experimental is yellow. At most of the points, the two curves conform to each other. Only for an electrical field between 11~12 kV/cm, the results of the two simulations differ. Because the measurement of the amplitude of vibration is a very difficult task, it is a good approach to trust the results produced by the numerical simulation.
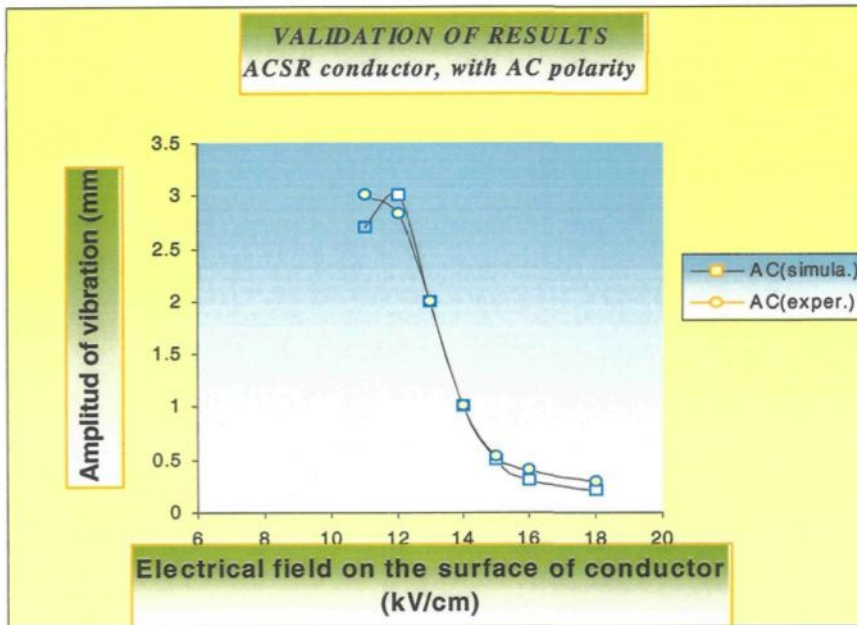
Figure 6-4: *ACSR conductor supplied by Alternative tension*

2) DC positive

The variation of the amplitude of vibration for the ACSR conductor under DC+ tension is shown in Figure 6-5. The blue curve shows the numerical simulation results and the brown curve the experimental results. For the superficial electrical field between 11~13 kV/cm, the numerical curve exactly conforms to the experimental curve. Then the two curves diverge but follow the same behavior with a decreasing bias and at the end hit each other when the superficial electrical field equals 18 kV/cm. As it is obvious from Figure 6-5 , for the lower voltages, the variation of the vibration amplitude is linear and predictable for the numerical simulation. It is also easier to measure for the experimental simulation. But as far as the applied voltage and consequently the superficial electrical field increased, the

nonlinearly increases and many different events interact (refer to chapter two for more details).

If we considered all the physical phenomena and the involved forces, it would make our numerical model too complex, which is not within the scope of this project. Therefore by neglecting some of the detailed data and by making a simpler numerical model, we are grateful to see the similar results as the experimental simulation.

3) DC negative

On Figure 6.6, the amplitude of vibration of the ACSR conductor supplied with the negative DC electrical fields is shown. The conductor is considered under rain precipitation rate above 25mm/h. The numerical curve is cyan and the experimental is yellow. At most of the points, the two curves conform to each other, which is interesting. As it was explained in the previous paragraph, for DC+, because of the physical shape and torsion factor of an ACSR conductor, the formation of the water drops and the reaction of the involved forces at high voltages are more complex and less predictable than for a smooth conductor. But it seems that the numerical model designed for the laboratory model, described in chapter four, is so close to the reality that it can be a good base for the numerical simulation of high voltage transmission lines.
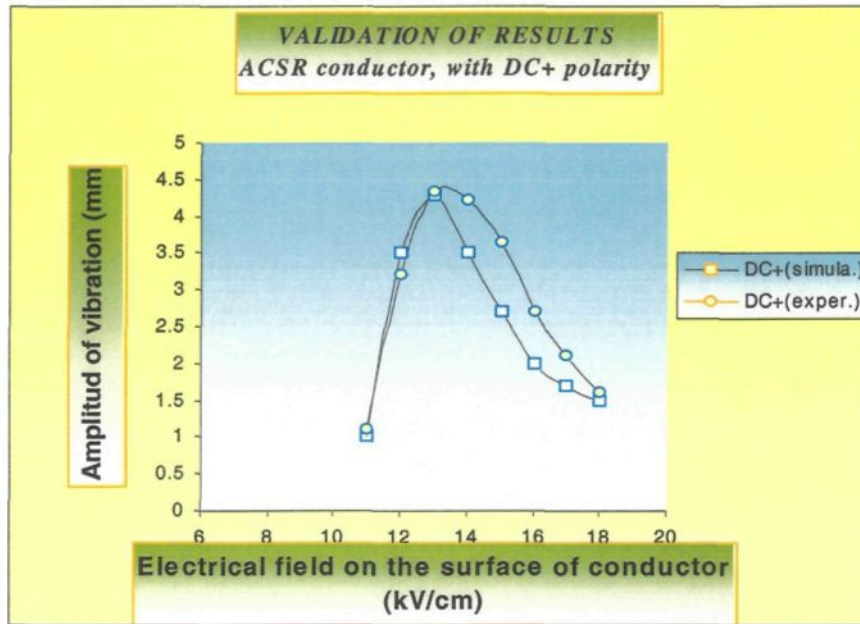
Figure 6-5: *ACSR conductor supplied by DC +*
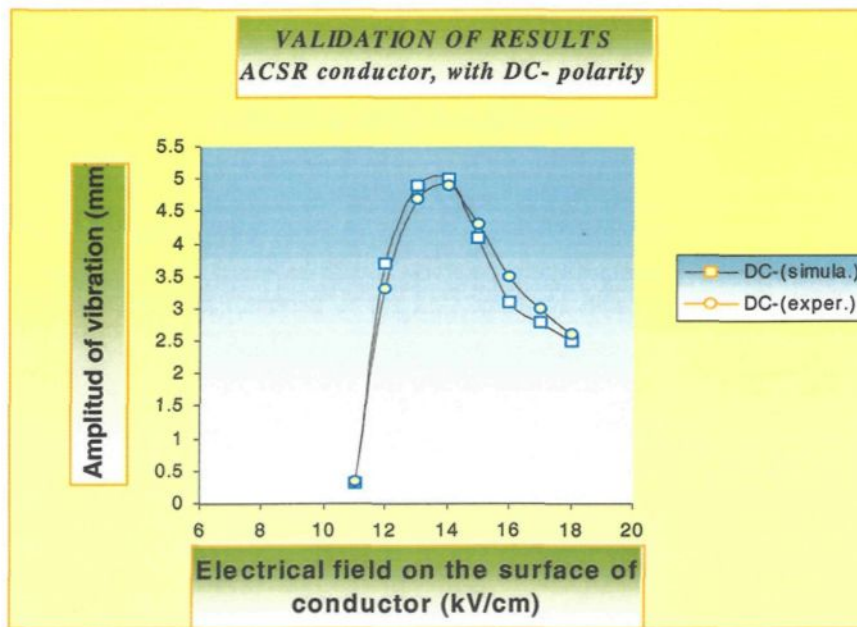
Figure 6-6: *ACSR conductor supplied by DC -*

CHAPTER 7

CONCLUSION

The results obtained from the research work presented in this thesis, which are related to the corona-induced vibration on a short conductor submitted to the artificial rain, leads to the following conclusion:

1. Shape of a suspended water drop under a high voltage conductor is related to the intensity and the polarity of the applied voltage. From the drop profiles shown in the appendix, it can be concluded that as far as the applied high voltage increases, the drop shape becomes more conic and the elongation of drops occurs faster, which lead to an earlier ejection. Each drop ejection applies an upward reaction force that leads to the vibration of the high voltage conductor. Therefore, it is mostly the increase in the number of drop ejection that increases the amplitude of vibration.

2. Shape of a suspended water drop under a high voltage conductor is related to the intensity of the precipitation. When the precipitation of rain falling over a high voltage conductor increases, the augmentation of the rain intensity accumulates the essential volume of water for ejection in a shorter period of time. This leads to a higher number of ejected water drops per cycle which consequences to a higher amplitude of vibration.

3. Characteristic of the drop volume is not related to the strength of the electrical field. But the variation of this parameter changes with respect to the intensity of the precipitation, for three different voltage polarities (AC, DC+, and DC-).

4. The following forces are involved in the force balance of a suspended water drop on a high voltage conductor which is under vibration: Gravity force, Inertia force, Electrostatic force, Tension of surface, Induced force by Corona. When sum of the

force induced by the corona and the adhesive force becomes larger than the sum of the three other forces (Inertia, gravity, and Electrostatic), the ejection of the water drop occurs.

5. Numerical simulation results show that the damping effect on a smooth conductor is more than an ACSR conductor. It means the damping of the amplitude of vibration is higher on a smooth conductor, a result that agree with the experimental results developed by Farzaneh [Farzaneh M., 1986, page 113].

6. Based on the Numerical results, the amplitude of vibration (induced by corona) of the hollow smooth conductor is maximum for an alternative electrical field and is minimum for negative DC. The changes of amplitude are the same for an electrical field between 13~14 kV/cm and is close to linear for all types of polarities. For the same value of electrical field supplied to the ACSR conductor, negative DC has the most amplitude of vibration and alternative has the less. These results can be explained by the fact that at the same applied voltage, corona activities in the air are usually stronger under negative fields than under positive fields because of the lower negative corona-onset voltage. The relatively low amplitude of the vibration under AC fields, compared to that under DC, may be attributed to the residual corona-space charge from the previous half cycle of each period of instantaneous voltage.

APPENDIX

DROP PROFILE FOR THE ACSR CONDUCTOR
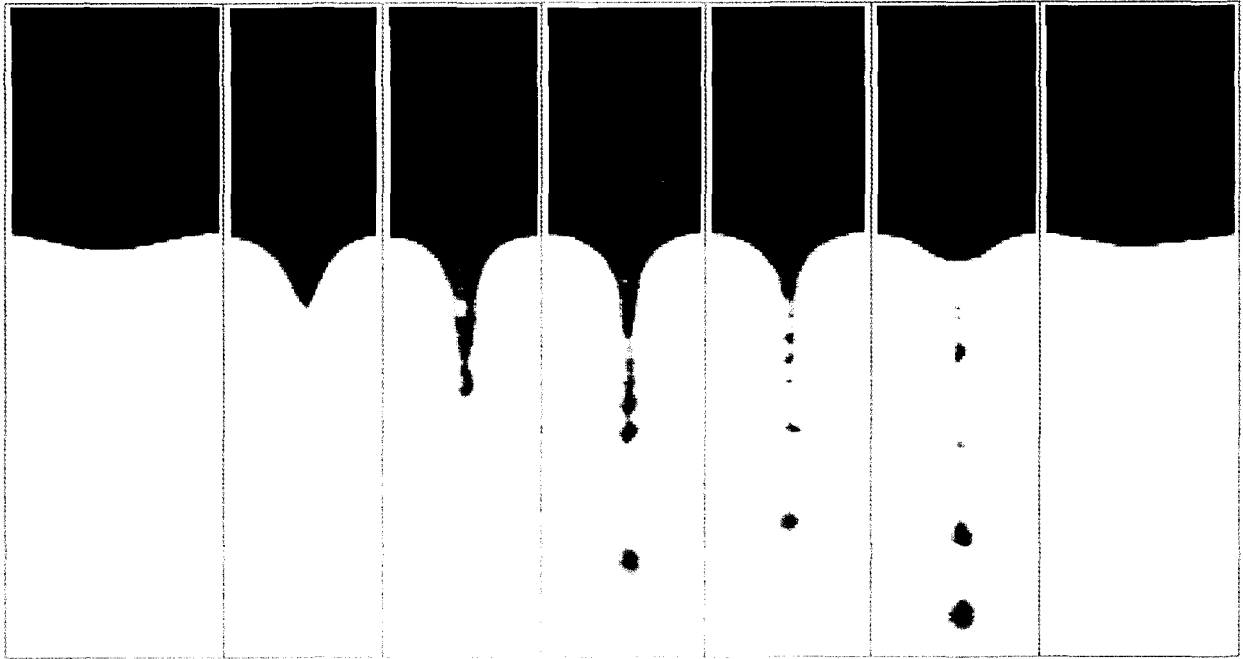
Figure A-1: *Drop profile of an ACSR conductor at 55 Kv AC and 170 cc/min water flow*
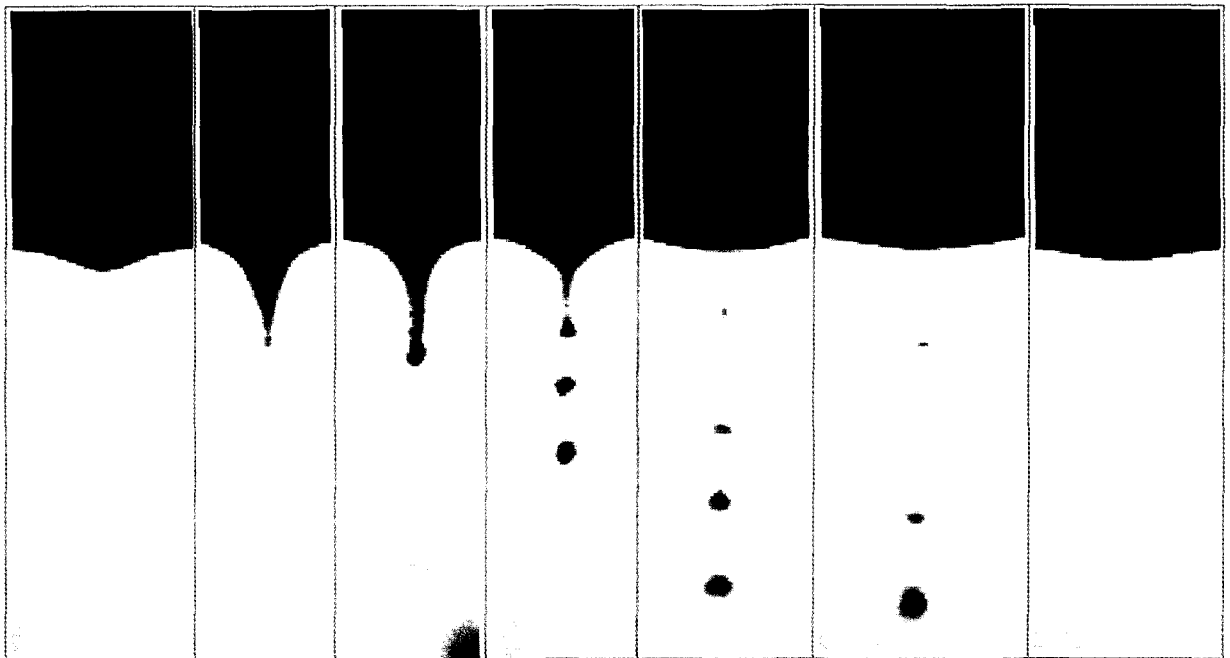

Figure A-2: *Drop profile of an ACSR conductor at 70 Kv AC and 612 cc/min water flow*
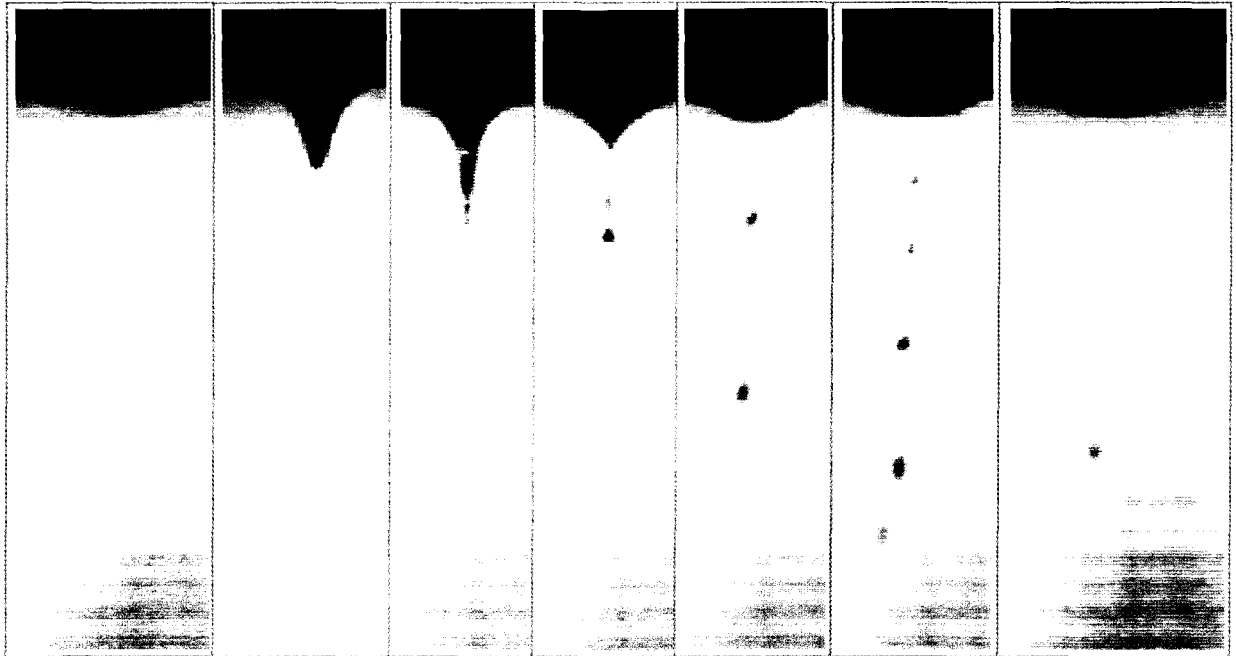
Figure A-3: *Drop profile of an ACSR conductor at 105 Kv DC+ and 612 cc/min water flow*
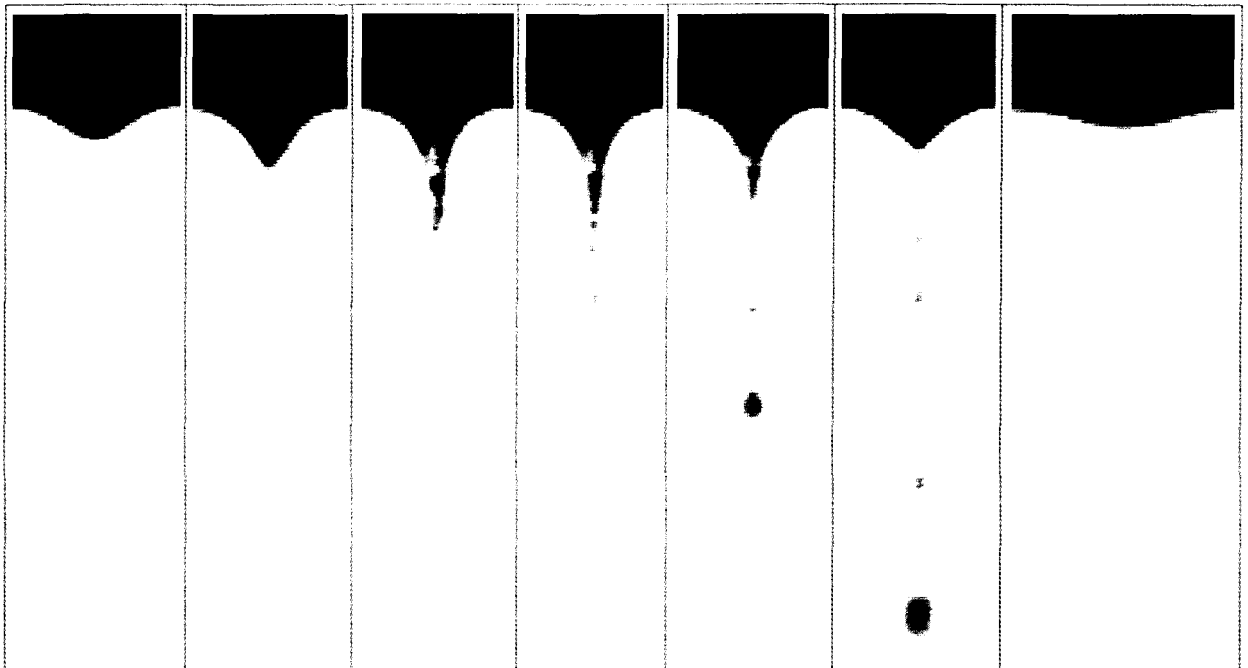
Figure A-4: *Drop profile of an ACSR conductor at 50 Kv DC+ and 90 cc/min water flow*
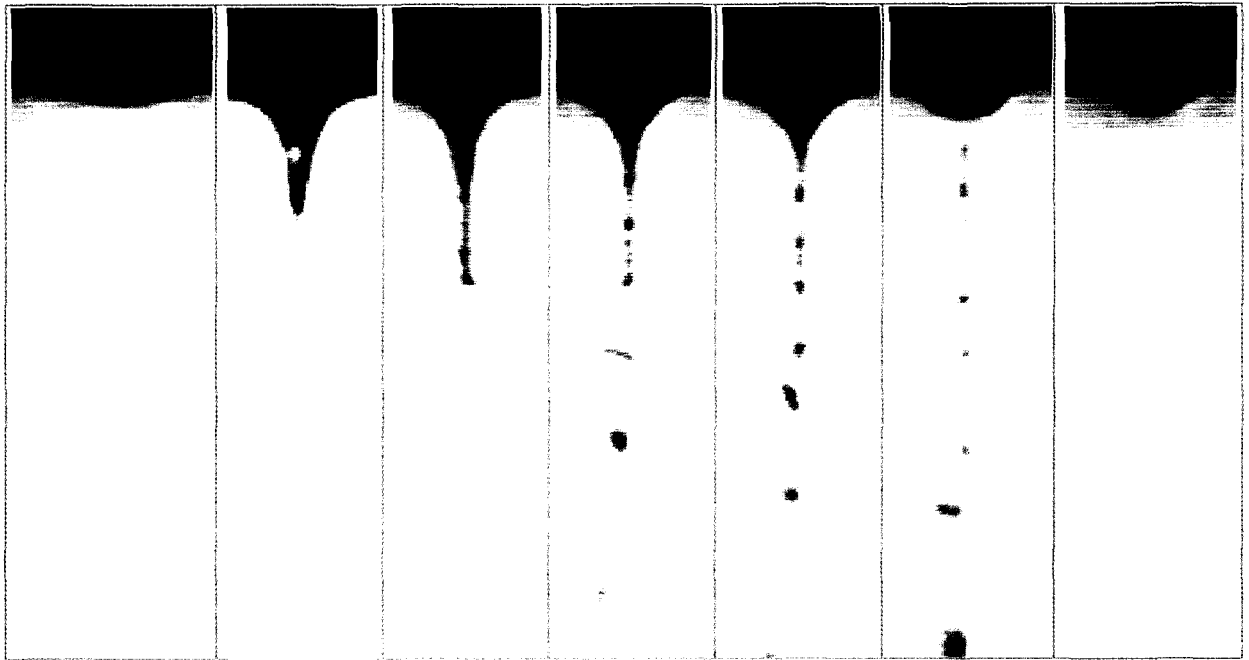
Figure A-5: *Drop profile of an ACSR conductor at 50 Kv DC- and 90 cc/min water flow*
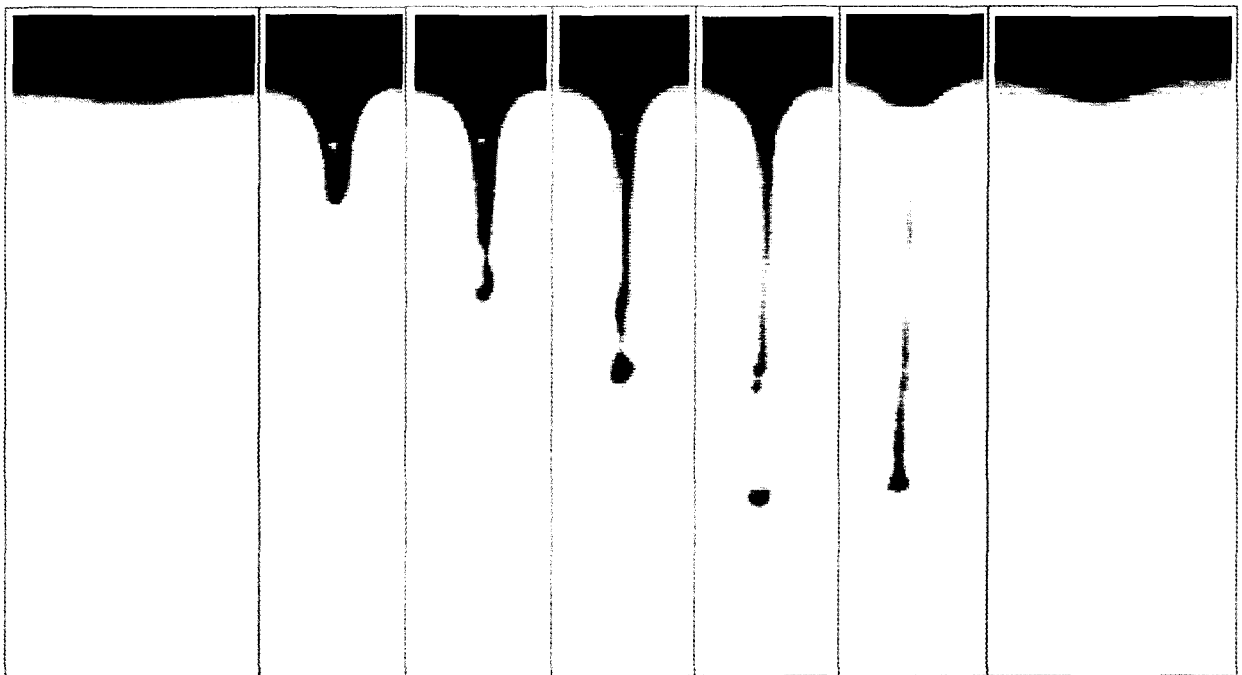
Figure A-6: *Drop profile of an ACSR conductor at 105 Kv DC- and 612 cc/min water flow*

References

1) Akazaki M., "Corona phenomena from water drops on smooth conductors under HDV", IEEE, January, 1965.

2) Akazaki M., Lin S.H., "Corona discharge from water drops dripping onto inner conductor of co-axial cylinder", Electrical Engineering in Japan, Vol. 88, no 5, 1968.

3) Biro O., Bardi I., Preis K., Renhart W., Richter K.R., "Finite element techniques applied to HV problems", 9th ISH 1995.

4) Burnett David S., "Finite Element Analysis", 1987 ISBN: 0-201-10806-2.

5) CIGRE (22nd committee) and IEEE (transport and distribution committee), "Guide pour les mesures d'auto- amortissement des conducteurs. ", Electra, no. 62, January 1979.

6) Deng H., Schaub B., "The equipotential method, a moving finite element method for electrostatic field calculations", 9th ISH 1995.

7) Farzaneh M., Phan L.C., "Vibration of high voltage conductors induced by corona from water drops or hanging metal points. ", IEEE, Sept. 1984.

8) Farzaneh M., "Contribution à l'étude des mécanismes des vibrations induites par effet de couronne", Ph.D. Thesis, university of Paul Sabatier in Toulouse, 1986.

9) Farzaneh M., Teisseyre Y., "Mechanical vibration of H.V. conductors induced by corona: roles of the space charge and ionic wind. ", IEEE, July. 1988.

10) Farzaneh M., "Effects of the intensity of precipitation and transverse wind on the corona induced vibration of H.V. conductors. ", IEEE, April 1992.

11) Farzaneh M., "Ingénierie de la haute tension", text book, UQAC, 1992.

12) Hamel M., "Influence de la variation de la température ambiante sur les vibrations induites par effet de couronne" , M.Sc. Thesis, University of Quebec in Chicoutimi, August, 1991.

13) Hara M., Hayata N., Akazaki M., "Basic Studies on ion flow electrification phenomena", Journal of Electrostatic, Vol. 4, pp. 349-365, 1978.

14) Hara M., Ishibe S., Akazaki M., "Corona discharge and electrical charge on water drops dripping from D.C. transmission conductors", Journal of Electrostatics, Vol. 6, pp. 235-257, 1979.

15) Hara M., Ishibe S., Sumiyoshitani S., Akazaki M., "Electrical corona and specific charge on water drops from a cylindrical conductor with HDC voltage.", Journal of Electrostatics, Vol. 8, pp. 239-270, 1980.

16) Hara M., Akazaki M., "Onset mechanism and development of corona discharge on water drops dripping from a conductor under high direct voltage. ", Journal of Electrostatics, Vol. 9, pp. 339-353, 1981.

17) Hara M., Yamashita T., "Microdischarge between charged water drop and objects", Journal of Electrostatic, Vol. 13, pp. 325-344, 1982.

18) Hokierti J., "Investigation of the electric field in a vicinity of a water drop adhering to a conductor. ", M.Sc. Thesis, University of Missouri-Rolla, Rolla, Mo., 1974.

19) Loeb L.B., "Fundamental processes of electrical discharges in gases", New York: John Wiley and Sons , 1939.

20) Loeb L.B. and al., "Pulses in negative point-to-plane corona", Physical Review, Vol. 60, 1941.

21) Loeb L.B., "Electrical coronas, their basic physical mechanism", Berkeley : University of California Press, 1963.

22) Maaroufi M., "Vibration induites par effet de couronne", Ph.D. Thesis, L'Ecole Mohammadia d'ingénieurs(EMI), Maroc , 1989.

23) Mark's Standard Handbook for Mechanical Engineers, Mc Graw Hill, 1978.

24) Migdalovici M.A., Sireteanu T.D., "A discrete method for modal analysis of overhead line conductor bundles", PVP-Vol. 330, Natural Hazard Phenomena and Mitigation, ASME 1996.

25) Nasser E., "Fundamentals of gaseous ionization and plasma electronics", New York: John Wiley and Sons, 1971.

26) Peek M.F., "Dielectric phenomena in high voltage engineering"`, McGraw- Hill, New York, 1915.

27) Shah K. S., Morgan J.D., "Analytical study and numerical simulation of high voltage transmission line oscillation induced by electrostatic forces", Ph.D. Thesis, University of Missouri-Rolla, Rolla, Mo., 1976.

28) Teisseyre Y., Farzaneh M., Bastien F., "Vent électrique produit par décharge de couronne sur les gouttes d'eau. " 54e Congrés de l'Acfas , University of Montreal, 1986.

29) Townsend J.S., "Electricity in gases", Oxford: Clarendon Press, 1915.

30) Wang J., Lilien J.L., "A new theory for torsional stiffness of multi-span bundle overhead transmission lines", PE-217-PWRD-0-11-1997, IEEE 1997.

31) Xin Li, Raghuveer M. R., Ciric I.R., "A new methode for solving ionized fields of unipolar HVDC lines including effect of wind. Part II: Iterative techniques and numerical tests", International Journal of Numerical Modeling, Vol. 10, p57-69, 1997.